(E86-10025 NASA-CR-176269) STUDY OF SPECTRAL/RADIOMETRIC CHARACTERISTICS OF THE THEMATIC MAPPER FOR LAND USE APPLICATIONS Final Report, 21 Sep. 1982 - 20 Jun. 1985 (Environmental Research Inst. of Michigan) G3/43
N86-16690 THRU N86-16694 Unclas 00025

164000-19-F

Final Report

STUDY ON SPECTRAL/RADIOMETRIC CHARACTERISTICS OF THE THEMATIC MAPPER FOR LAND USE APPLICATIONS

21 September 1982 — 20 June 1985

WILLIAM A. MALILA
MICHAEL D. METZLER

SEPTEMBER 1985

Original photography may be purchased
from EROS Data Center
Sioux Falls, SD 57198

Contract NAS5-27346
NASA Goddard Space Flight Center
Greenbelt Road
Greenbelt, Maryland 20771

ENVIRONMENTAL
RESEARCH INSTITUTE OF MICHIGAN
BOX 8618 • ANN ARBOR • MICHIGAN 48107

NOTICES

Sponsorship. The work reported herein was conducted by the Environmental Research Institute of Michigan under Contract NAS5-27346 for the National Aeronautics and Space Administration, Goddard Space Flight Center, Greenbelt, MD 20771. Contracts and grants to the Institute for the support of sponsored research are administered through the Office of Contracts Administration.

Disclaimers. This report was prepared as an account of Government sponsored work. Neither the United States, nor the National Aeronautics and Space Administration (NASA), nor any person acting on behalf of NASA:

(A) Makes any warranty expressed or implied, with respect to the accuracy, completeness, or usefulness of the information, apparatus, method, or process disclosed in this report may not infringe privately owned rights; or

(B) Assumes any liabilities with respect to the use of, or for damages resulting from the use of any information, apparatus, method, or process disclosed in this report.

As used above, "person acting on behalf of NASA" includes any employee or contractor of NASA, or employee of such contractor, to the extent that such employee or contractor of NASA or employee of such contractor prepares, disseminates, or provides access to any information pursuant to his employment or contract with NASA, or his employment with such contractor.

Availability Notice. Request for copies of this report should be referred to:

National Aeronautics and Space Administration
Scientific and Technical Information Facility
P.O. Box 33
College Park, Maryland 20740

Final Disposition. After this document has served its purpose, it may be destroyed. Please do not return it to the Environmental Research Institute of Michigan.

TECHNICAL REPORT STANDARD TITLE PAGE

1. Report No.	2. Government Accession No.	3. Recipient's Catalog No.
164000-19-F		

4. Title and Subtitle	5. Report Date
Study of Spectral/Radiometric Characteristics of the Thematic Mapper for Land Use Applications	October 1985
	6. Performing Organization Code

7. Author(s)	8. Performing Organization Report No.
William A. Malila and Michael D. Metzler	164000-19-F

9. Performing Organization Name and Address	10. Work Unit No.
Environmental Research Institute of Michigan P.O. Box 8618 Ann Arbor, MI 48107	11. Contract or Grant No. NAS5-27346
12. Sponsoring Agency Name and Address	13. Type of Report and Period Covered
National Aeronautics and Space Administration Goddard Space Flight Center Greenbelt, MD 20771	Final Report 21 Sep 1982 - 20 Oct 1985
	14. Sponsoring Agency Code

15. Supplementary Notes

Mr. Harold Oseroff (Code 902) served as Technical Officer and Mssrs. Brian Markham and James Irons (Code 923) served as Science Representatives for NASA/GSFC.

16. Abstract

This is a summary report of an investigation conducted in support of the Landsat 4/5 Image Data Quality Analysis (LIDQA) Program. Results of engineering analyses of radiometric, spatial, spectral, and geometric properties of the Thematic Mapper systems are summarized; major emphasis was placed on the radiometric analysis. Details of the analyses are presented in appendices which contain three of the eight technical papers which were produced during this investigation; these three, together, describe the major activities and results of the investigation.

17. Key Words	18. Distribution Statement
Radiometric Calibration Landsat-4, Landsat-5 Thematic Mapper Data Quality Multispectral Scanner Subsystem Information Content Imaging Noise	Initial distribution is listed at the end of this document.

19. Security Classif. (of this report)	20. Security Classif. (of this page)	21. No. of Pages	22. Price
UNCLASSIFIED	UNCLASSIFIED	49 + iii	

Report No. 164000-19-F

Final Report
21 September 1982 — 20 June 1985

on

Study of Spectral/Radiometric Characteristics of the Thematic Mapper for Land Use Applications

under

Contract NAS5-27346

with

NASA Goddard Space Flight Center
Greenbelt Road
Greenbelt, Maryland 20771

Submitted by

Environmental Research Institute of Michigan
P.O. Box 8618
Ann Arbor, Michigan 48107

Prepared by: William A. Malila
William A. Malila
Principal Investigator

Michael D. Metzler
Co-Investigator

Approved by: Robert Horvath
Robert Horvath
Manager, Information Processing Department

September 1985

Table of Contents

D1

N86-16691

Final Report

STUDY OF SPECTRAL/RADIOMETRIC CHARACTERISTICS OF THE THEMATIC MAPPER FOR LAND USE APPLICATIONS

1. OBJECTIVES

The objectives of this investigation were to quantify the performance of the Thematic Mapper, as manifested by the quality of its image data, in order to suggest improvements in data production and to assess the effects of the data quality on its utility for land resources applications. The effort was to include analyses of radiometric, spatial, spectral, and geometric effects, with primary emphasis on radiometric effects.

This effort was part of the Landsat 4/5 Image Data Quality Analysis (LIDQA) program sponsored by the NASA Goddard Space Flight Center.

2. ACCOMPLISHMENTS, CONCLUSIONS, AND RECOMMENDATIONS

Engineering analyses were conducted to assess image data quality of the Landsat-4 and -5 Thematic Mappers (TMs). Macroscopic studies addressed trends and characteristics of full frames of data, while "microscopic" studies assessed differences between individual detector responses. Raw data, radiometrically corrected (Type A) data, and fully corrected (Type P) data were analyzed, as well as special calibration data. In addition, coincident data from the TM and the Landsat Multispectral Scanner Subsystem (MSS) were compared. A summary of these analyses is given below and many of the details are presented in Appendices A-C.

1. Landsat-4 and -5 Thematic Mapper (TM) data were generally found to be of high quality and exhibited several improvements over corresponding Multispectral Scanner Subsystem (MSS) data.
   a. The spatial resolution of the TM is substantially better than that of the MSS (nominally 30 m vs 82 m) and provided images with much greater spatial detail.
   b. The radiometric quantization of TM is finer (256 levels vs 64 levels at the spacecraft); however, part of this gain was used for increased dynamic range in channels rather than all being used for improved radiance resolution.
   c. The greater number of spectral bands of TM (seven vs four) allows sampling of additional spectral regions and provides increased information

about the scene.

2. Detailed analyses were conducted which discovered several noticeable but relatively low-amplitude radiometric data anomalies or artifacts and addressed methods for removing them or reducing their effects:
   a. Signal Droop/Rise Along Scan Lines
      i) The mean signal level of each of the Primary Focal Plane bands (Bands 1-4) was seen to decay or "droop" across the scan during daylight data acquisition, and to "rise" with time during nighttime data collection.
      ii) The magnitude of the effect was found to be relatively small (maximum effect of less than 4% of mean signal level), but it does produce image banding between scan directions near frame edges.
      iii) An exponential decay model with a time constant equivalent to approximately 1000 pixels was found to fit the observed "droop/rise"; it could be used to correct data for this effect, but the correction would have to be computed separately for each pixel.
   b. Scan-correlated Level Shifts
      i) The mean output signal level of most detectors was found to shift up or down with a fixed amplitude but at essentially random intervals. These "scan-correlated level shifts" fell into two patterns for Landsat 4, named Type 4-1 and Type 4-7 after the spectral bands most strongly displaying each effect, and one pattern for Landsat 5, Type 5-3. All detectors belonging to a particular pattern shifted in unison, although some might shift up while others shifted down.
      ii) Essentially all detectors were affected, but with different amplitudes. The phase and amplitude relationships were found to be very stable, with magnitudes being as great as two video quantum levels (DN) in the worst case, and less than 0.5 DN in most other cases.
      iii) Procedures for removing the level-shift artifact from the image data were developed and demonstrated; they use 20-48 samples of calibration data which are not generally available to Landsat data users. Therefore corrections for this artifact should be incorporated in the TIPS (Thematic Mapper Image Processing System) processor.
   c. Quantization Step Size
      i) The quantization step sizes in the A/D converters on the Thematic Mappers (both Landsat 4 and Landsat 5) were unequal in size, resulting in uneven distribution of data within the signal space spanned.
      ii) Errors introduced by this artifact are small, typically one quantum level or less.
      iii) The resampling process used to produce fully corrected (Type P) data both masks the presence of this artifact and precludes a correction for it.
   d. Histogram Gaps (Empty Bins)
      i) The application of gains greater than unity to the raw signals during radiometric correction resulted in occasional "empty bins" in

the individual detector histograms.

ii) Although unappealing from an aesthetic sense, the result is a natural consequence of stretching the quantized data.

iii) No correction is possible; evidence of the effect is masked in fully corrected (Type P) data by the detector-equalization and resampling processes.

e. Coherent Noise

i) Very low amplitude (< 0.25 DN) coherent noise was observed at a frequency of approximately 400 Hz.

ii) Although the source of this noise was not definitely determined, its effect was judged to be minimal.

f. Thermal (Band 6) data were found to have a full-range temperature span of 200°K to 340°K instead of the advertised 260°K to 320°K; the correct range is indicated in the calibration parameters provided in the digital tape headers.

3. Radiometric comparisons were made using data from simultaneous acquisitions.

a. Simultaneous coverage by Landsat 4 and Landsat 5 Thematic Mappers occurred during orbit adjust maneuvers shortly after the launch of Landsat 5 and allowed direct radiometric comparison of the two sensors to be made.

i) Relationships were established between data from the two sensors; gain differences as large as 14 percent were noted in calibrated data.

ii) Low-level clipping was observed in the radiometrically corrected Landsat-5 data for Bands 5 and 7, but not in raw data.

iii) A continued monitoring of system performance and data calibration would be valuable to many users of Landsat data.

b. Simultaneous Landsat-4 TM and MSS coverages allow comparisons of the radiometry from those two sensors as well; one such scene pair was analyzed.

i) High degrees of correlation were found; relationships to convert single spectral bands of TM data into MSS-equivalent data were developed.

ii) Spectrally transformed features (Tasselled-Cap Brightness and Greenness) were compared; Greenness values were almost perfectly correlated, but Brightness values exhibited some differences (correlation coefficient of 0.75).

iii) TM data were observed to have higher spectral dimensionality than the MSS data.

c. Information theoretic measurement techniques were developed and applied to simultaneous TM and MSS data. Analyses of the data volumes realized by each sensor relative to the information potential of the sensors were made, and the greater information content of TM data from an agricultural scene was quantified.

3. PUBLICATIONS AND PRESENTATIONS

In addition to the ten Quarterly Status and Technical Progress Reports, and presentations at Investigator Workshops and Symposia, eight technical papers dealing with efforts under this contract have been published in journals and symposium proceedings. They are listed below. Copies of Papers 4, 7, and 8 are included as Appendices A, B, and C, respectively. These three papers, together, describe the major activities and results of the investigation.

1. Metzler, M.D., and W.A. Malila, "Scan-angle and Detector Effects in Thematic Mapper Radiometry," in *Proc. Landsat−4 Early Results Symp.*, NASA Goddard Space Flight Center, Greenbelt, MD, February 1983.
2. Metzler, M.D., and W.A. Malila, "Radiometric Characterization of Thematic Mapper Full-Frame Imagery," in *Proc. SPSE/APS Conf. on Techniques for Extraction of Information from Remotely Sensed Images*, Rochester, NY, August 1983.
3. Malila, W.A., D.P. Rice, and M.D. Metzler, "Radiometric Analyses of Landsat-4 Digital Image Data," in *Proc. of the PECORA VIII Symp.*, Sioux Falls, SD, Octoberr 1983.
4. Malila, W.A., M.D. Metzler, D.P. Rice, and E.P. Crist, "Characterization of Landsat-4 MSS and TM Digital Image Data," *IEEE Trans. Geosc. Remote Sensing*, Vol. GE-22, no. 3, pp. 243-251, May 1984.
5. Malila and W.A., M.D. Metzler, "Thematic Mapper Radiometric Characterization," in *Proc. 1984 Purdue/LARS Symp. on Machine Processing of Remotely Sensed Data*, W. Lafayette, IN, June 1984.
6. Malila, W.A., "Information Theoretic Comparisons of Original and Transformed Data from Landsat MSS and TM," in *Proc. 18th International Symp. on Remote Sensing of Environment*, Paris, France, October 1984.
7. Metzler, M.D. and W.A. Malila, "Characterization and Comparison of Landsat-4 and Landsat-5 Thematic Mapper Data," *Photogrammetric Engineering and Remote Sensing*, Vol. 51, no. 9, pp. 1315-1330, September 1985.
8. Malila, W.A., "Comparison of the Information Contents of Landsat TM and MSS Data," *Photogrammetric Engineering and Remote Sensing*, Vol. 51, no. 9, pp. 1449-1457, September 1985.

APPENDIX A

Characterization of Landsat-4 MSS and TM Digital Image Data

Characterization of LANDSAT-4 MSS and TM Digital Image Data

WILLIAM A. MALILA, MEMBER, IEEE, MICHAEL D. METZLER, DANIEL P. RICE, AND ERIC P. CRIST

Abstract—Engineering analyses conducted to assess image data quality are described and results are presented for the Landsat-4 Multispectral Scanner (MSS) and Thematic Mapper (TM). Also, coincident data from the two sensors are compared. Macroscopic studies addressed trends and characteristics of full frames of data, while "microscopic" studies assessed differences between individual detector responses. Raw data, radiometrically corrected data, and fully corrected data were analyzed, as well as special calibration data.

The Landsat-4 MSS was found to produce data of high quality, comparable to previous Landsats, except for a low-level coherent noise effect which is unique to the current sensor. Radiometric relationships between Landsat-2 and -3 MSS's and the Landsat-4 MSS were established through empirical analysis of simultaneously acquired data.

The TM was found to produce image data of very good spatial resolution and overall good radiometric data quality, showing improvements over MSS. Radiometric equalization of detector responses was found to be close to the theoretical limit of quantization error, except for two relatively low-amplitude artifacts. One is a difference in response that depends on the direction of mirror scan. This produces scan-angle effects superimposed on scene-related effects. The second is a tendency for level shifts to occur between mirror scans at random times but with correlations between detector responses. Two forms or patterns of level shift were identified, corresponding to four system noise states. Preliminary correction models and/or procedures have been developed and recommended for further evaluation.

In a comparison of coincident coverages of one agricultural scene, high degrees of correlation were found between MSS signals and those from corresponding TM bands. Very high correlation also was observed between spectrally transformed Greenness variables for the two sensors. Lower correlation was observed for Brightness.

Keywords—Remote Sensing, Landsat-4, Multispectral Scanner, Thematic Mapper, Digital Image Processing, Radiometric Calibration, Coherent Noise, Scan Effects, Level Shifts, Detector Equalization, Spatial Resolution.

I. INTRODUCTION

THE JULY 1982 launch of Landsat-4 and its two sensors represented both a continuation and a new beginning in the remote sensing of Earth resources [1]. A second decade of satellite imaging with the Multispectral Scanner (MSS) is underway. Its 80-m spatial resolution is fine enough to resolve many natural features and land-use details in both rural and urban settings. Coupled with the spectral information of its four bands, many applications have evolved and developed during the past decade. A new era of sensing with refined spatial resolution (30 m) and expanded spectral coverage (7 bands) has begun with the orbiting of the Thematic Mapper (TM) [2], [3]. Although telemetry problems have restricted the acquisition of data by the Landsat-4 TM, sufficient data have been analyzed to excite investigators about its increased information potential and evoke anticipation for the forthcoming launch of Landsat-D' and the second TM sensor.

This paper describes results from engineering studies of the characteristics of digital image data from the two Landsat-4 sensors [4]-[7]. These studies are part of the Landsat-4 Image Data Quality Analysis program (LIDQA) which was organized and sponsored by the National Aeronautics and Space Administration (NASA), Goddard Space Flight Center (GSFC), Greenbelt, MD [8]. Control of the MSS sensor and system was transferred from NASA to the National Oceanic and Atmospherics Administration (NOAA) in January 1983, while the TM system is planned to remain on experimental status until a later date. The studies described here were focussed on the radiometric characteristics of the MSS and TM, with limited consideration of spectral and spatial properties. Studies such as these are desirable so that subsequent investigators and users of data will have verification of the system's performance and knowledge of any artifacts, without the necessity of each conducting his or her own detailed analysis. Also, NASA uses the results of internal and external LIDQA investigators to make improvements in product generation procedures.

We believe that continuity of an operational remote sensing system, like the Landsat MSS, has at least two aspects: a) continued availability of high-quality data and b) consistent interpretability of signal amplitudes and spectral features extracted from those data.

Both sensors scan linear arrays of detectors perpendicular to their ground track in order to achieve coverage of the scene beneath. If detectors within a band are not perfectly calibrated with respect to each other (i.e., equalized), image banding or striping results and extra variability or noise is introduced into the statistical descriptions (e.g., signatures) of signals from specific scene classes. Similarly, if the noise associated with each detector channel were to significantly exceed design specifications, the utility of the data collected by the system would be diminished. Also, reduced dynamic range could degrade data utility.

In addition, the sensor response should be consistent and preferably constant as a function of scan angle, position along track, and days in orbit, to permit unambiguous and consistent information extraction and interpretation. For MSS, this extends to a need either to match the radiometric calibration of the preceding Landsat MSS sensors or to establish relation-

Manuscript received December 2, 1983; revised December 27, 1983. This work was supported by the National Aeronautics and Space Administration (NASA), Goddard Space Flight Center, Greenbelt, MD under Contracts NAS5-27254 and NAS5-27346.

The authors are with the Environmental Research Institute of Michigan, Ann Arbor, MI 48107.

0196-2892/84/0500-0177$01.00 © 1984 IEEE

ships for appropriately adjusting coefficients and thresholds in affected algorithms and procedures that were developed for earlier data. For TM, which employs bidirectional scanning, one would not want response to depend on scan direction.

Continuity in spectral response is important to MSS. It also is desirable to compare the spectral information content of TM to that of MSS in order to assess both the extent to which the same information can be extracted from TM and any increase in information that may be available because of the additional spectral bands in TM.

II. Approach and Method

Both macroscopic and microscopic analyses were conducted of digital computer-compatible-tape (CCT) data from both sensors. Data from several stages of the ground data processing procedure were analyzed, including raw data, radiometrically corrected data, fully corrected data, and calibration data, as available.

The macroscopic analyses were designed to assess trends within spectral bands over the full 185 × 185-km frames of data. First, histograms and statistical measures (e.g., means and standard deviations) of signal amplitudes were computed for each band. Where available, radiometrically corrected and fully corrected data were examined and compared. Selected scatterplots were made of data in pairs of bands and signal correlations computed. MSS responses from selected scene classes also were compared qualitatively with expectations based on our experience with previous Landsats.

Second, scan-angle effects were investigated by averaging columns of pixels down the entire frame, plotting the results (amplitude versus pixel number or scan angle) for each band, and analyzing these average scan lines. Third, to explore the other image dimension, down-track profiles (amplitude versus scan line number) were computed, one for each band, by averaging all pixels (or a systematic sample) on each line to obtain a single average value for each scan line. Fourth, to study any scan direction effects in TM, average scan lines were computed for each band, separately for each of the two scan directions. Computer plots and listings of the computed average scan lines and down-track profiles were produced and analyzed.

Finally, to compare radiometric calibration between the Landsat-4 MSS and Landsats-2 and -3, opportunities for simultaneous acquisitions were identified and a few pairs of scenes were acquired for analysis. Simultaneous acquisition was possible on selected dates at selected locations due to the 16-day cycle of Landsat-4 and the 18-day cycle of Landsats-2 and -3.

The microscopic analyses were designed to assess differences between individual detector responses before and/or after equalization within each spectral band (6 detectors for each MSS band, 16 for each TM reflective band, and 4 for the TM thermal band). They also were designed to examine noise characteristics by detector, both down-track and along the scan line. Many of the analyses conducted on spectral band values were repeated for each individual detector to provide data for comparison. Detector histograms and related statistics, together with the down-track profiles, permitted assessment of the ground systems' success in equalizing detector responses. A unique aspect was our analysis of nighttime TM data from the reflective channels. Fourier analysis of down track profiles also was used to assess the success of equalization and to detect the presence of periodic banding and striping effects. A Fast Fourier Transform (FFT) technique adapted from [9] was used.

A coherent noise effect was visually apparent in MSS data. Fourier analysis of individual scan lines, selected throughout the frame, was accomplished using the FFT procedure. The frequencies of anomalously large components were identified and their amplitudes measured from the FFT analysis output.

Geometric and spatial characteristics also were considered. The pixel lengths of MSS scan lines were examined and compared in radiometrically corrected data (CCT-AT) from an Eastern U.S. scene acquired when TM was operating and a Western U.S. scene acquired when TM was off. For comparison of MSS and TM and for illustration of spatial-resolution effects on one's ability to resolve fine detail, an appropriate scene (North Carolina, Path 14/Row 36) for which simultaneous MSS and TM coverage existed was selected. Scan line traces (amplitude versus pixel number) were plotted in a 3-D projection to permit comparison and to illustrate differences. Quantitative comparison was based on computed signal variances within individual fields.

Finally, a limited comparison of spectral responses from MSS and TM was made for the same simultaneously acquired scene. Spatial registration was accomplished by means of pixel shifts based on control points identified in the two images; an accuracy of approximately one pixel was achieved. Groups of four TM pixels were averaged for comparison with their associated MSS pixels. Correlations were computed between MSS and comparable TM bands. Also, correlations were computed between spectrally transformed features, namely Brightness and Greenness, defined for the two sensors [10]. The MSS transformation was equivalent to the Tasseled-Cap Transformation of Kauth and Thomas [11], while the TM transformation is an analogous one developed by Crist and Cicone [12]. The reader is referred to [12] for a more detailed discussion of the spectral characteristics and spectral information content of TM.

III. Data Sets

Table I identifies the 9 MSS frames which were analyzed part of this study; they were acquired during the first four months of Landsat-4 operation. The 6 TM frames analyzed are listed in Table II; they represent the first six months of operation. Radiometrically corrected (CCT-AT) digital data tapes were the primary data sources for our MSS studies, supplemented by fully corrected imagery. Raw data (CCT-BT) and radiometrically corrected data (CCT-AT) were the primary inputs for our TM studies, with added analyses of fully (geometrically as well as radiometrically) corrected data (CCT-PT) and calibration data (CCT-ADDS). The CCT-BT and CCT-ADDS are special engineering products not generally available to users. The MSS data were products of the Multispectral Scanner Image Processing System (MIPS), while the TM data were processed through the interim processing system (SCROUNGE) established at NASA/GSFC.

TABLE I
MSS ANALYSIS DATA SET

Geographic Location	Landsat	Path/Row	Date	Frame
S. Carolina (inland)	4	17/36	29 Sep 82	40075-15271
California (Imperial Valley)	4	39/37	23 Sep 82	40069-17433
N. Carolina (coast)	4	14/36	24 Sep 82	40070-15084
N. Carolina (coast)	3	15/35	24 Sep 82	31664-15070
"	4	14/35	24 Sep 82	40070-15081
New England	3	14/30	22 Dec 82	31753-14591
"	4	13/30	22 Dec 82	40159-15010
New Mexico	2	34/37	9 Nov 82	22848-16571
"	4	32/37	9 Nov 82	40116-17005

TABLE II
TM ANALYSIS DATA SET

Geographic Location	Path/Row	Date	Frame Number	Scene Type
Arkansas	23/35	22 Aug 82	40037-16034	Agriculture, some clouds, water
Iowa	27/30	3 Sep 82	40049-16262	Agriculture, clear skies
North Carolina	14/36	24 Sep 82	40070-15084	Agriculture, much cloud, water
Cape Cod	11/31	8 Dec 82	40145-14492	Low radiance, clouds, much water
Georgia	116/207	24 Dec 82	40161-02481	Nighttime
Grand Bahamas	14/42	14 Jan 83	40182-15125	Water, clouds

IV. MSS ANALYSIS RESULTS [4], [5]

A. Landsat-4 MSS Data Quality

1) Qualitative Comparisons with Data from Preceding Landsats: Scatterplots and statistics derived from data from the first two scenes listed in Table I were examined, in both comprehensive samples from the entire frames and samples from distinct scene classes. Fig. 1 displays the MSS3-versus-MSS2 data dispersion of the comprehensive sample from the Imperial Valley scene; spectral regions occupied by four scene classes are outlined on the figure. Water is represented by low signals in all bands, while sand is bright in all bands. Clouds were so bright as to cause signal saturation (Level 127) at the prevailing solar illumination angle of 47° (elevation). Also, agricultural data can be seen to fill out a roughly triangular shape (a rotated "tasseled cap" shape). These observations are generally true also for data we had examined previously from Landsats-1-3.

In addition, we compared data from the simultaneously acquired Landsat-3 and Landsat-4 data pair over the coast of North Carolina. Image displays and general statistics showed good correspondence.

2) Detector Equalization and Quantization Effects: Visual examination of photographic images and other displays of MSS data revealed evidence of stripes and bands caused by incomplete detector equalization, in areas of nearly uniform signals (such as water bodies and barren plains). Signal means computed for each detector in five such areas of the Imperial Valley scene are presented in Table III. Among the six detector means for each band, the standard deviation was generally less than 0.3 counts, while 0.88 counts was the largest difference. A more comprehensive estimate of residual banding and striping throughout the first two MSS frames listed in Table I came from the FFT analysis of down-track profiles. Evidence of radiometric disturbances, which did not appear to be associated with ground phenomena, were observed at spatial wavelengths of 2, 3, and 6 pixels. The largest calculated average deviation from the mean of the 6 detectors was 0.27 ± 0.05 count for the South Carolina frame. This result is in good agreement with the Imperial Valley values in Table III.

The detector equalization algorithm used by the production system for full-frame MSS data sets [13] was examined to see if any further improvement seemed possible. The algorithm carries out signal decompression (Bands 1-3 only), calibration wedge normalization, and detector histogram equalization using a single transformation of received satellite samples to determine final count levels. A separate transformation is computed for 600-scan-line segments within the 2400-scan-line frame, and then is interpolated to each 200-scan-line sub-segment. The result is a pattern of full count-level bins with occasional empty ones, a pattern which differs among detectors due to both their differing responses and the correction process. Examination of this pattern for a series of 200-scan-line sub-segments showed the expected gradual change from one segment to the next, and indicated that the algorithm worked as intended.

A very important limit on accuracy of this equalization algorithm is not one of measuring differences or determining corrections, but rather one of translating corrected values to nonfractional count levels. The theoretical rms error of this truncation process is 0.29 [14], which is similar to the error magnitudes reported above. That is, the current correction algorithm cannot be improved much if any without dealing with the truncation error problem. This error could be reduced somewhat (per radiance unit) by using more numeric precision, for example by spreading the signal values over the range 0-255 instead of the current 0-127. However, the analog-to-digital conversion process in the satellite and its similar assignment to nonfractional values during its six-bit quantization can cause minor but uncorrectable quantization effects which will be most noticeable in relatively uniform areas.

3) Coherent Noise: A careful visual examination of imagery from Landsat-4 MSS revealed a diagonal striping pattern, particularly in areas of nearly uniform radiance. Our FFT analysis of this noise pattern on selected scan lines distributed throughout the first two Landsat frames of Table I revealed that the noise existed at a dominant spatial wavelength of about 3.6 pixels along scan, as illustrated by Fig. 2, and was present in all bands. The frequency corresponding to the observed dominant wavelength is approximately 28 kHz. The wavelength was slightly different (3.57 compared to 3.59) for the two frames, but was consistent (± .001) within each frame. In one frame (South Carolina), two other wavelengths appeared somewhat consistently, namely the wavelengths of 2.02 and

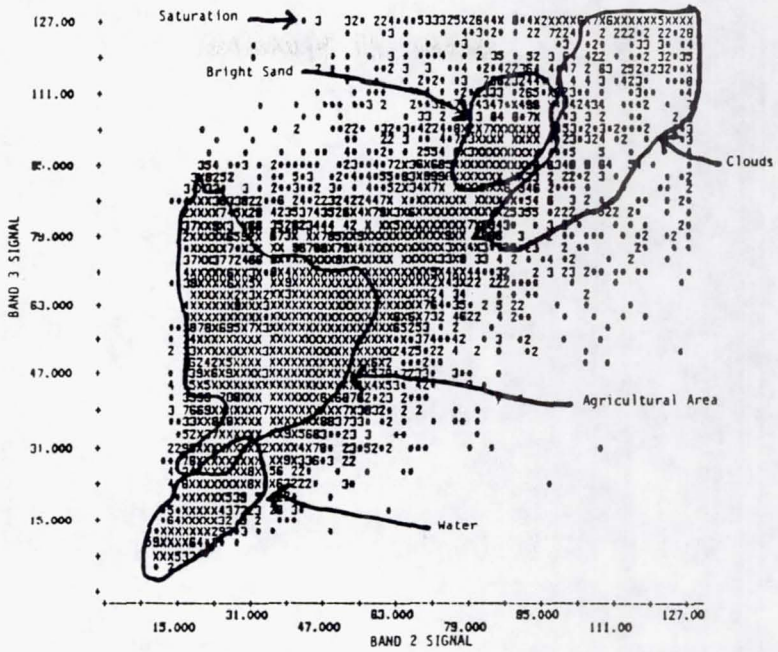

Fig. 1. MSS spectral distribution of scene classes from the Imperial Valley, CA scene.

TABLE III
DETECTOR AVERAGES FOR 5 AREAS IN ONE LANDSAT-4 MSS FRAME (Imperial Valley, CA)

Detector	1	2	3	4	
1	23.01	21.08	36.80	14.44	
2	23.29	21.00	36.91	14.41	
3	22.94	21.10	36.94	14.53	
4	23.23	21.04	37.31	14.62	Highlands
5	23.25	20.97	37.18	14.43	
6	23.31	21.03	37.15	14.70	
Std. Dev. =	.16	.05	.19	.12	
1	33.08	35.51	53.86	19.03	
2	33.38	35.78	54.18	19.09	
3	33.41	36.06	54.32	18.99	
4	33.32	36.10	54.22	18.80	Agricultural
5	33.31	35.86	53.60	18.81	
6	33.08	35.69	53.75	18.91	
Std. Dev. =	.15	.22	.29	.12	
1	62.23	76.10	84.14	25.73	
2	62.11	76.76	84.25	25.62	
3	62.10	76.08	84.54	25.84	
4	61.42	76.01	84.04	25.89	Sand
5	61.78	75.88	83.81	25.84	
6	61.99	76.23	83.88	25.63	
Std. Dev. =	.30	.31	.27	.12	
1	20.79	13.65	10.09	2.43	
2	21.02	13.69	9.88	2.35	
3	20.64	13.70	9.91	2.21	
4	20.73	13.52	9.59	2.27	Water
5	20.26	13.37	9.84	2.07	
6	20.81	13.90	10.22	2.30	
Std. Dev. =	.25	.18	.22	.12	
1	51.62	61.55	69.43	22.10	
2	51.77	61.82	69.17	22.27	
3	51.58	61.58	69.30	22.44	Bright Shallow
4	52.16	61.68	69.52	22.53	Valley
5	51.28	62.07	69.31	21.97	
6	51.67	61.79	69.56	22.05	
Std. Dev. =	.29	.19	.15	.22	

4.63 pixels, but these and other smaller peaks in both frames were not analyzed in detail. The magnitude of the sine-wave component at the primary peak was computed and tabulated for the group of scan lines that was processed. This information, presented in Table IV, shows that the rms magnitude of the noise did not exceed one count in the worst band (MSS1).

NASA scientists now suspect that this effect may be due to a coherent noise source in a power supply. Based on the magnitudes described above, we consider this effect to be a relatively minor source of error, in spite of its nuisance effect on image appearance and its possible effects on classification results for spectrally similar classes. Nevertheless, it would be desirable to eliminate this noise source from future sensors.

4) Geometric Distortion: In carrying out the MSS radiometric analysis described above, a significant geometric distortion was noted in some CCT-AT tapes used in the analysis. This distortion was characterized by adjacent groups of 6 scan lines (each group comprising one mirror sweep) being displaced relative to one another, as illustrated in Fig. 3. The magnitude of the displacement varied up to 6 pixels and decreased to zero at the left side of the image, indicating that the distortion is a line length variation. We found that this distortion was absent or much reduced in one scene (Imperial Valley) taken when the Thematic Mapper sensor was not operating.

For further analysis of the scenes acquired with the TM operating, we implemented a linear line stretch correction, based on the position of end-of-scan codes in each scan line, which we understand is equivalent to the correction used by the EROS Data Center (EDC) to produce the geometrically corrected Landsat-4 CCT-PT tapes. This correction substantially improved the geometric correspondence between paired Landsat-3 and -4 datasets. As Fig. 3 shows, this correction restored the river (vertical band of dark symbols) to its proper contiguous course. Thus fully corrected data from EDC should exhibit little if any residual effect, but users of CCT-AT tapes should expect to find displacements.

B. Between-Satellite Radiometric Calibration of MSS

1) Matched Datasets: Three loci of frame centers in the U.S. were identified along which ground paths of Landsats-3 and -4 coincided sufficiently to permit similar view directions

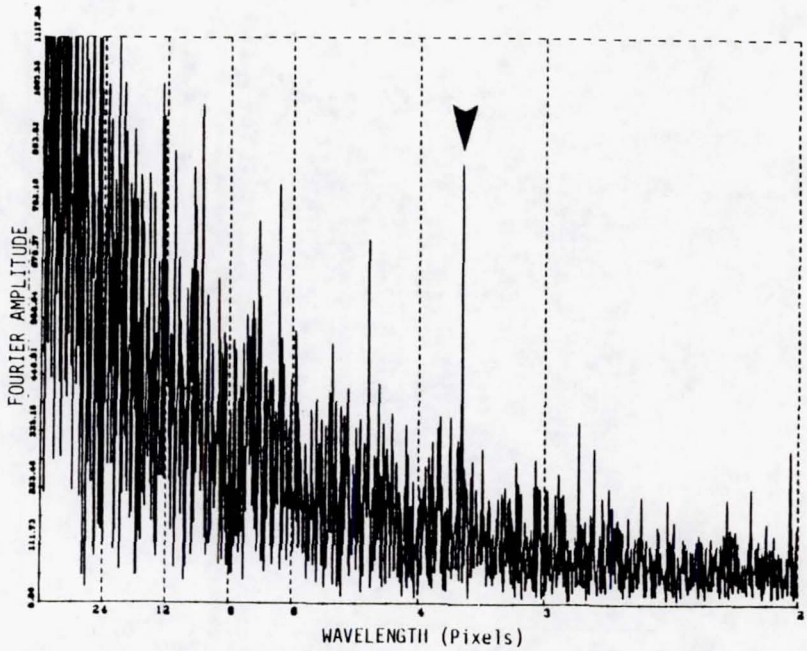

Fig. 2. Along-scan Fourier transform showing MSS coherent noise peak at wavelength 3.6 (South Carolina, Scan Line 2117. MSS3).

TABLE IV
AVERAGE MAGNITUDE OF MSS COHERENT NOISE EFFECT

Band	Magnitude (counts)
1	0.75 ± .11
2	0.52 ± .09
3	0.56 ± .10
4	0.50 ± .10*

*This Band 4 value has been scaled to reflect the calibration of data produced on or after 20 October 1982.

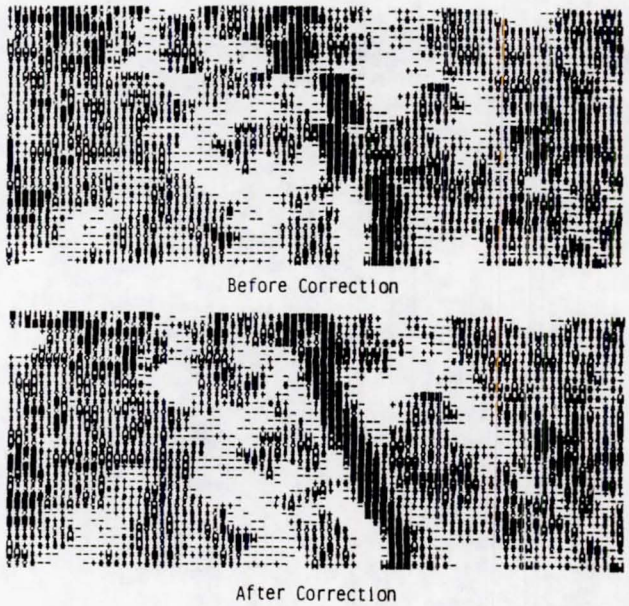

Fig. 3. Line-length variation in Landsat-4 MSS CCT-AT tapes (South Carolina).

to scene locations. Fig. 4 shows one along the East Coast, one in the central U.S. and the other near the West Coast. The two outside loci would allow repeated coincident coverages every 144 days (144 being the least common multiple of 18 and 16), but coverages no closer than one day apart were possible for the central locus. Several of the identified potential coincident-coverage datasets were requested and approved for collection. After losses due to cloud cover and acquisition problems were incurred, collection of coincident Landsat-3 and -4 data was successful on 5 dates in the U.S. Furthermore, although Landsat-2 has not been collecting MSS data operationally since February 1982, it was brought to our attention that a coincident Landsat-2/Landsat-4 dataset was collected in November 1982 and we were provided a copy for analysis [15]. The coincident-coverage datasets we analyzed are listed in Table I; regression relationships are presented in the next section for the New England pair for Landsats-3 and -4 and for the New Mexico pair for Landsats-2 and -4.

2) Empirical Regression Relationships: From the New England Landsat-3/4 data set, 60 relatively large and uniform polygonal areas were carefully identified and located in both frames. These areas were selected to provide as wide a spectral range as possible. Table V presents empirically derived linear regression coefficients for the following equation:

$$[\text{Landsat-3 Signal}] = \text{Gain} * [\text{Landsat-4 Signal}] + \text{Offset}.$$

Note that very high R^2 values and small standard errors on the order of one-half count were achieved. Also included in the table are coefficients based on published pre-launch calibration values. These pre-launch gains are seen to be approximately 10 percent lower than the empirical values, for data processed by the EROS Data Center (EDC) between October 20, 1982 and April 1, 1983; small adjustments in EDC coefficients were made on April 1, 1983 [16].

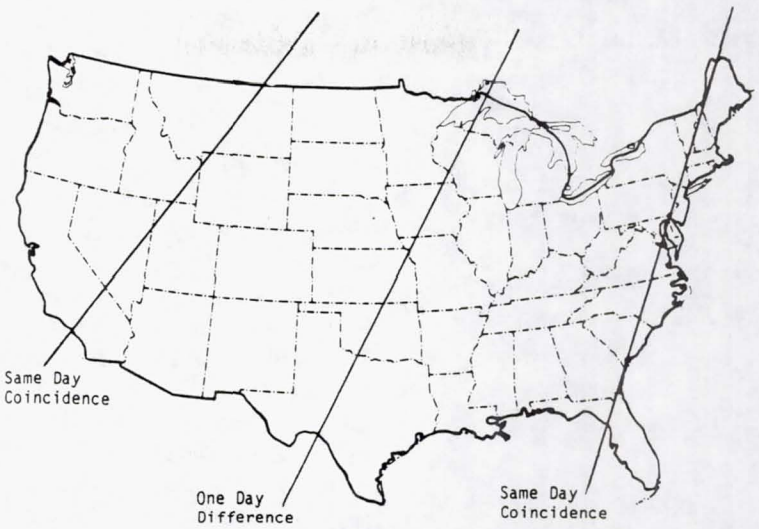

Fig. 4. Loci of frame centers with potential coincident coverage by Landsats-3 and -4.

TABLE V
EMPIRICAL LANDSAT-4 to -3 CALIBRATION COEFFICIENTS

Scene	Band	Gain	Offset	SE*	R^2
New England	1	1.018	-1.614	0.52	0.996
	2	1.112	0.018	0.45	0.999
	3	0.9096	-0.463	0.53	0.999
	4	1.148	-0.421	0.53	0.998
Prelaunch Calibration**	1	0.894	-1.00		
	2	1.000	0.722		
	3	0.863	0.870		
	4	1.026	2.34		

Notes:

*SE = standard error in signal counts

**This information represents carefully conducted ground measurements taken before launch of each satellite, along with appropriate scaling of the data to account for ground processing algorithm coefficients.

***The values in this table assume EROS Data Center (EDC) processing of the data between 20 October 1983 and 1 April 1983; EDC sources should be consulted for coefficient adjustments on and after 1 April 1983.

Relationship:

Landsat 3 = Gain x (Landsat 4) + Offset

TABLE VI
EMPIRICAL LANDSAT-4 to -2 CALIBRATION COEFFICIENTS

Scene	Band	Gain	Offset	SE	R^2
New Mexico	1	0.8766	-0.592	0.96	0.973
	2	1.0124	2.187	1.12	0.989
	3	0.8796	1.699	0.97	0.995
	4	1.1002	-2.629	0.59	0.997
Prelaunch	1	0.894	-2.988		
Calibration	2	1.035	-1.494		
	3	0.863	-1.740		
	4	1.026	-0.334		

Relationship:

(Landsat 2) = Gain x (Landsat 4) + Offset

See Notes under Table V.

To contrast the effects of using various forms of data correction, potential errors were calculated for dark, intermediate, and bright areas. Between 2 and 12 counts of error would occur, using an Euclidean count difference measure, if Landsat-4 data were to be used directly as a substitute for Landsat-3 data. If pre-launch measurements of calibration were used to correct the difference, the error would still fall between 3 and 9 counts, an insubstantial improvement. Thus use of the empirical relationships in Table V is recommended, with the caution that any additional changes in ground processing coefficients should be taken into account.

Table VI presents an analogous set of coefficients for Landsats-2 and -4, based on 15 polygonal areas. Note that the standard errors are approximately twice as large as for Landsats-3 and -4, indicating less accuracy. Besides being fewer in number, the polygons used for Landsat-2/4 were more difficult to locate, and there were patterns of haze variation that could possibly have caused some differences when coupled with a 2.9° difference in view angle and a 4-min difference in acquisition time.

V. COMPARISON OF MSS AND TM

A. General Characteristics and Specifications

Table VII summarizes the major differences between MSS and TM specifications, indicating ways in which TM (and/or Landsat-4) represents extensions of the spatial, spectral, temporal, and radiometric characteristics of the MSS of Landsats 1-3. Specific details are readily available from [1]-[3] or related papers in this issue.

These improved specifications offer the potential for greater information gathering capacity, given appropriate information extraction techniques. LIDQA engineering studies are directed at assessing the extent to which particular performance goals have been met and searching out any unwanted system characteristics that might interfere with extraction of the information.

TABLE VII
EXTENSIONS OFFERED BY TM/LANDSAT-4 BEYOND THE CHARACTERISTICS OF MSS/LANDSATs 1-3

1)	SPATIAL SPECIFICATIONS
	a) 30m vs. 80 m resolution
	b) Improved platform stability (Landsat 4 vs. Landsats 1-3)
2)	SPECTRAL SPECIFICATIONS
	a) Narrower spectral bandwidths
	b) Additional spectral regions (Blue-green, intermediate IR, thermal IR)
3)	TEMPORAL SPECIFICATIONS (LANDSAT 4 VS. LANDSATS 1-3)
	a) Repeat cycle of 16 vs. 18 days
	b) Repeat coverage of overlap zone of 7 or 9 days vs. next day
4)	RADIOMETRIC SPECIFICATIONS
	a) Improved signal-to-noise
	b) Increased dynamic range (8 bits vs. 6 bits)

B. Comparisons of Coincident Data

1) Site Description: The site selected for our limited, but direct, comparison of MSS and TM data [10] is a private agricultural holding along the coast of North Carolina. This recently cleared area of 18 000 hectares is divided into square-mile blocks by improved two-lane gravel roads. Each block is bordered by drainage ditches and is divided into 16 strip fields (each 100 m wide) by a series of 3-m-wide drainage ditches. Fields of soybeans, corn, and fescue at various stages of development were present. An unusual amount (nearly 20 cm) of rain had fallen just prior to the overpass data Sept. 24, 1982. MSS2 and TM3 images of the site are presented in Fig. 5.

2) Spatial Comparison: The images of Fig. 5 very clearly illustrate the improved resolving power of the TM system. Field edges, roads, and other features are sharp and well defined. In many of the large square-mile fields (those having little vegetation present), the patterns of drainage ditches and narrow strip fields are clearly seen in the TM image but not in the MSS. Another graphical display of the differences in resolving power of the two systems is presented in Fig. 6. A computer plotter produced a horizontal line for each pixel at a height proportional to its amplitude. Lines connecting the levels of adjacent pixels give rise to a random staircase-like pattern for each scan line illustrated. Multiple lines crossing Test Region 1 (outlined on Fig. 5) are displayed in a 3-D perspective and clearly show the strip-field pattern for TM but not for MSS. Histograms and signal variances substantiated and quantified this difference.

3) Spectral Comparison: Three TM spectral bands (TM2, TM3, and TM4) span nearly the same spectral region as the 4 MSS bands. The spectral diversity of the test site provided a good data set for computing correlations between data values from these two sets of bands. Results are shown in Table VIII. Correlations of TM4 were about 0.97 and 0.99 between MSS3 and MSS4, respectively, and much lower and of opposite sign for the two visible bands, as would be expected due to vegetation characteristics. TM3 was most highly correlated with MSS2 (0.98), and quite well correlated with MSS1. Finally, TM2 was well correlated (0.91) with both MSS1 and MSS2. Table VIII also contains correlations between Brightness and Greenness variables computed for the two data sets. The Greennesses are very highly correlated (0.99), while the Brightnesses are less well correlated (0.75), a result which warrants further investigation and is likely due in part to the added information of the intermediate IR bands in TM Brightness.

VI. TM ANALYSIS RESULTS [6], [7]

A. General Characteristics of TM Data

1) Signal Histograms and Dynamic Range: Signal values over the full 0-255 signal range have been observed in all 6 reflective bands, with clouds frequently causing saturation. However, in a cloud-free, primarily agricultural scene (Iowa), we found narrow concentrations of signals in all bands but TM4 and TM5 which had somewhat broader distributions (see Fig. 7).

Fig. 8 presents several TM4 signal histograms to illustrate other TM characteristics. In parts (a), (b) and (c), responses from all detectors are grouped together. A ragged histogram shape is evident for the raw data of part (a), the result of unequal step sizes in the analog-to-digital converter of the sensor. After radiometric correction, part (b), the levels of individual detectors are shifted with respect to each other and the raggedness is decreased. Finally, the cubic-convolution interpolation process used in geometric correction results in a smooth histogram, part (c), for the fully corrected data. Parts (d) and (e) are for a single detector, with part (d) again displaying the A/D step size variation. When the radiometric correction process involves a stretching of the signal range (gain > 1.0), occasional gaps (empty levels) are created in the histogram as a direct result of the quantized, integer nature of the signal values, as shown in part (e). Because the detectors have slightly different gains and offsets, these empty levels are not evident in the histogram for the entire band, part (b), although they will still be present for individual detectors in CCT-AT data.

2) Detector Equalization and Down-Track Profiles: Just as for MSS, detector equalization within TM bands was found to be close to the theoretical limit of quantization. Residual differences in CCT-AT detector means were evident in corresponding CCT-PT scan-line means (down-track profiles) and in imagery.

In addition to the residual differences in detector means, we discovered another down-track artifact: very low frequency, scan-related noise in the form of level shifts that occurred in the mean values of individual detector means [6]. Other investigators also reported related observations [17]. This artifact is discussed in more detail in Section VI-C.

3) Scan-Angle Effects: Upon examination of plots of average scan lines (amplitude versus scan angle (pixel number)), it was found that values near the Western edge of the scene were substantially higher than those near the Eastern edge, as shown in Fig. 9. The effect, more pronounced in the short wavelength and thermal bands, can be attributed to sun-view geometry and a combination of atmospheric, bidirectional-reflectance, and shadowing effects. Previous modeling work has predicted atmospheric scan angle effects similar to those observed here [18], [19]. A plot of model results derived by us from the data set of Dave [20] is illustrated in Fig. 10. As the wavelength increases, atmospheric effects are reduced and the reflectance effects become the drivers of observed trends.

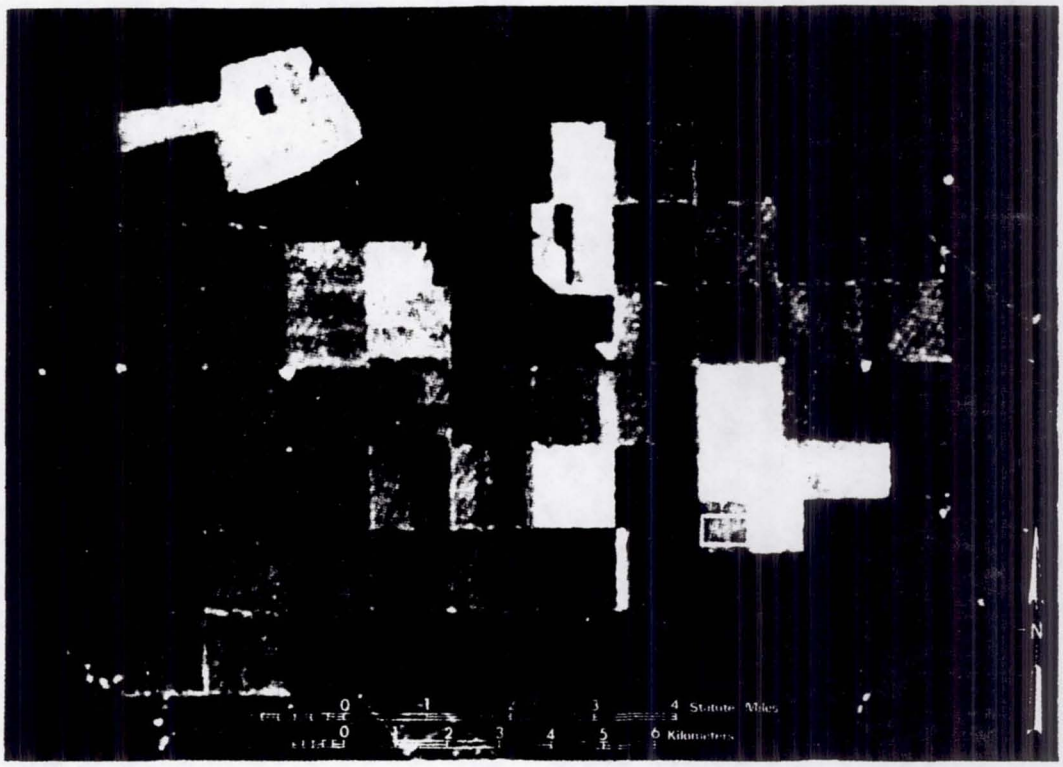

(a)

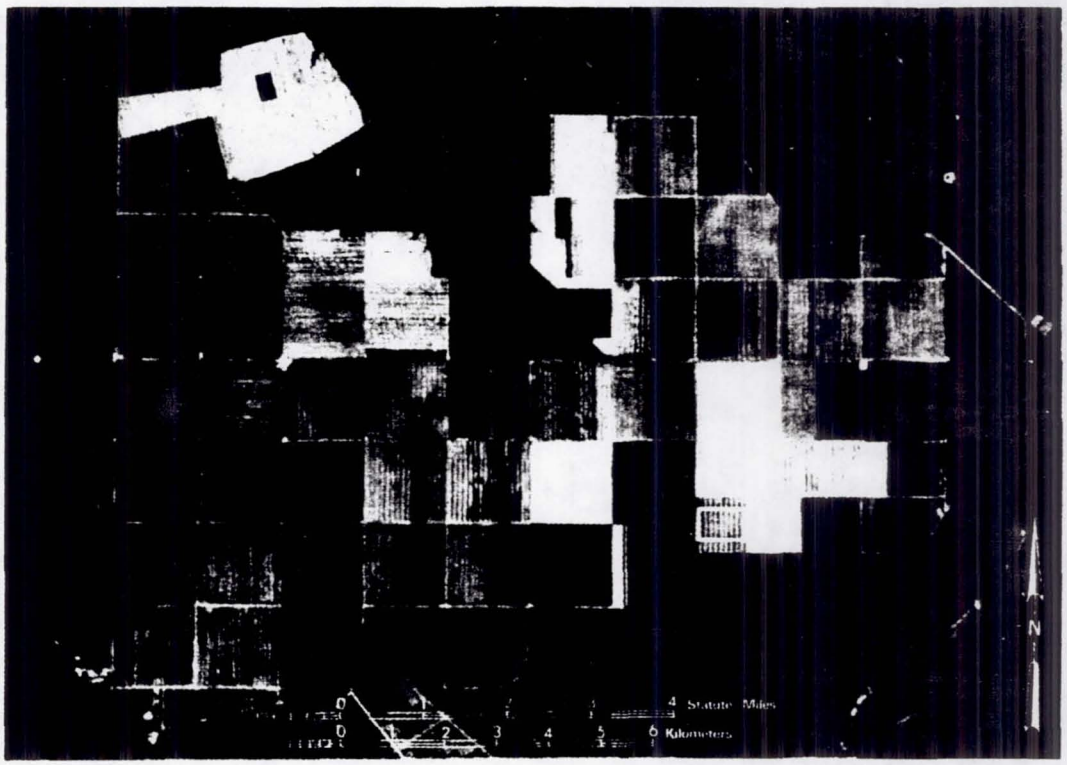

(b)

Fig. 5. Comparison of MSS and TM images of agricultural scene (1 identifies the region plotted in Fig. 6). (a) MSS Image. (b) TM Image.

Shading and view direction contribute to the observed thermal responses.

In addition to the expected scene-related scan-angle effects described above, we discovered a sensor-related scan-angle effect that is associated with the direction of mirror scan [6]. This artifact is discussed in more detail in Section VI-B.

B. Scan-Direction Artifact and Correction Model

1) Description of Artifact: From plots of average scan lines for the two scan directions, we found a slight but consistent anomaly, the difference between West and East edge values was greater for forward (W-E) scans than for reverse (E-W) scans. Fig. 11 illustrates the results for Bands TM1 and TM6

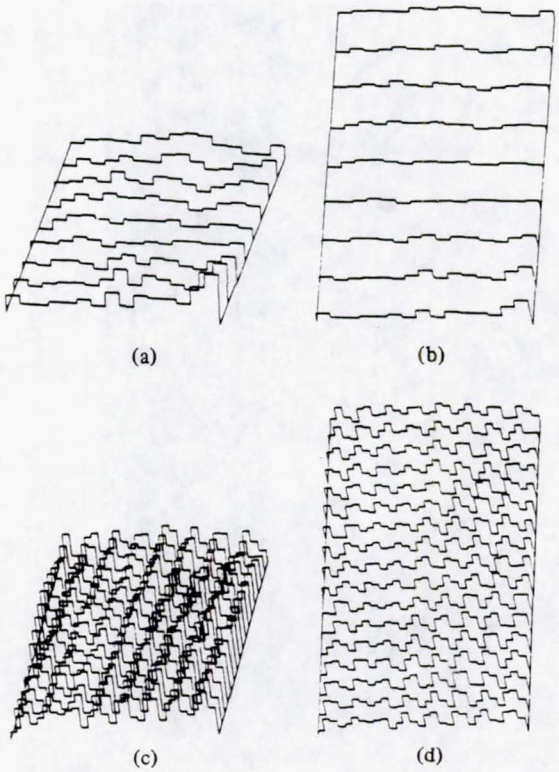

Fig. 6. Geometric resolution comparison–Test Region 1: BRIGHTNESS. (a) MSS-Perspective #1. (b) MSS-Perspective #2. (c) TM-Perspective #1. (d) TM-Perspective #2.

TABLE VIII
CORRELATION RESULTS FOR MSS AND TM
(Averaged Pixels)

a)	Original Band Values				
	TM 2	.909	.907	-.209	-.356
	TM 3	.881	.975	-.455	-.574
	TM 4	-.391	-.586	.972	.986
		MSS 1	MSS 2	MSS 3	MSS 4
b)	Tasseled-Cap Features				
	TM Brightness/MSS Brightness				.747
	TM Greenness/MSS Greenness				.990

for the Iowa frame, but it was observed in other bands as well. The previously described scan-angle effect is still dominant, but it appears that a systematic droop of signal values occurs during the active scan. This tends to increase the overall scan-angle effect for forward scans and reduce it for reverse scans for the reflective bands, being most pronounced in TM1. Thus 16-detector-wide swaths (approximately 17 lines on CCT-PT tapes and images) can differ from neighboring swaths by opposite amounts at the two frame edges, while little if any of this effect will be present at frame center.

In the thermal band, TM6, the swaths are four detectors wide and, as seen in Fig. 11, the scan-direction artifact for the September 1982 scene was markedly different from that of Band TM1 and the other reflective bands. This unique thermal band artifact has been observed in other scenes and by other investigators [23]. The problem is under study by NASA.

2) Correction Model for Band TM1: In order to charac-

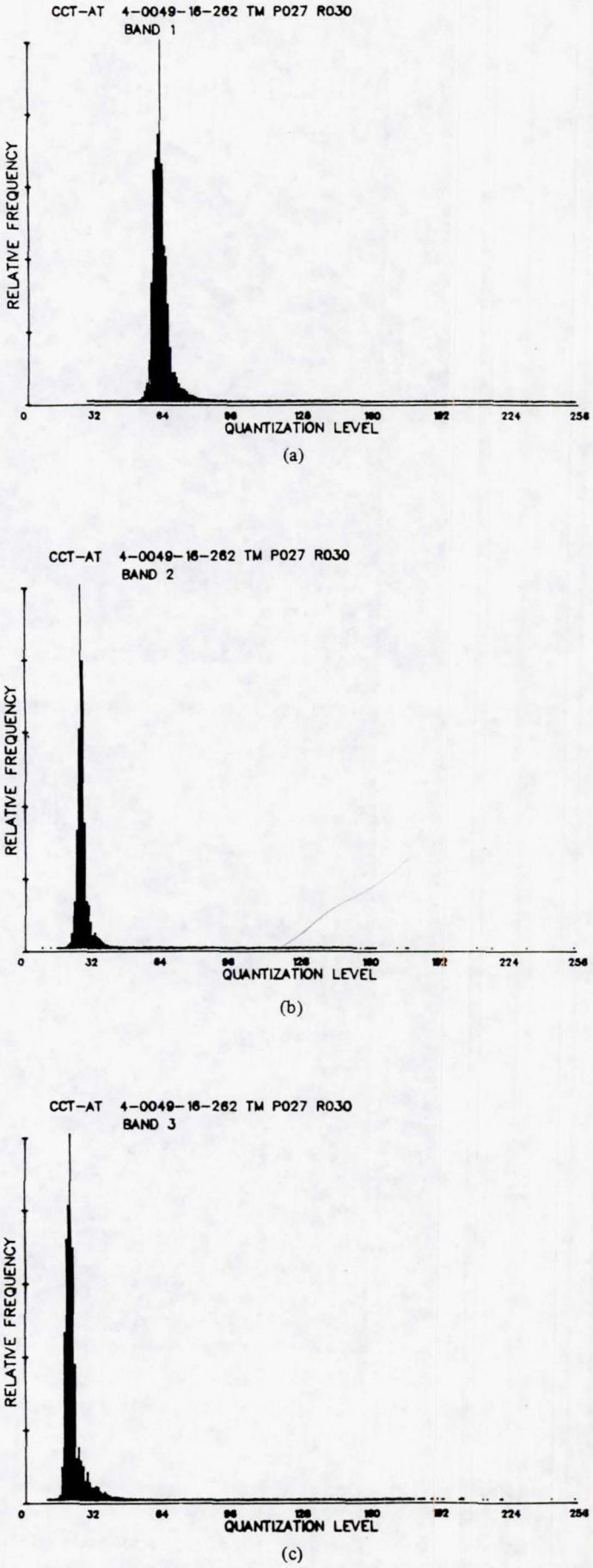

Fig. 7. Full-frame histograms for TM (Frame 40049-16262). (a) Band 1. (b) Band 2. (c) Band 3. (d) Band 4. (e) Band 5. (f) Band 6. (g) Band 7.

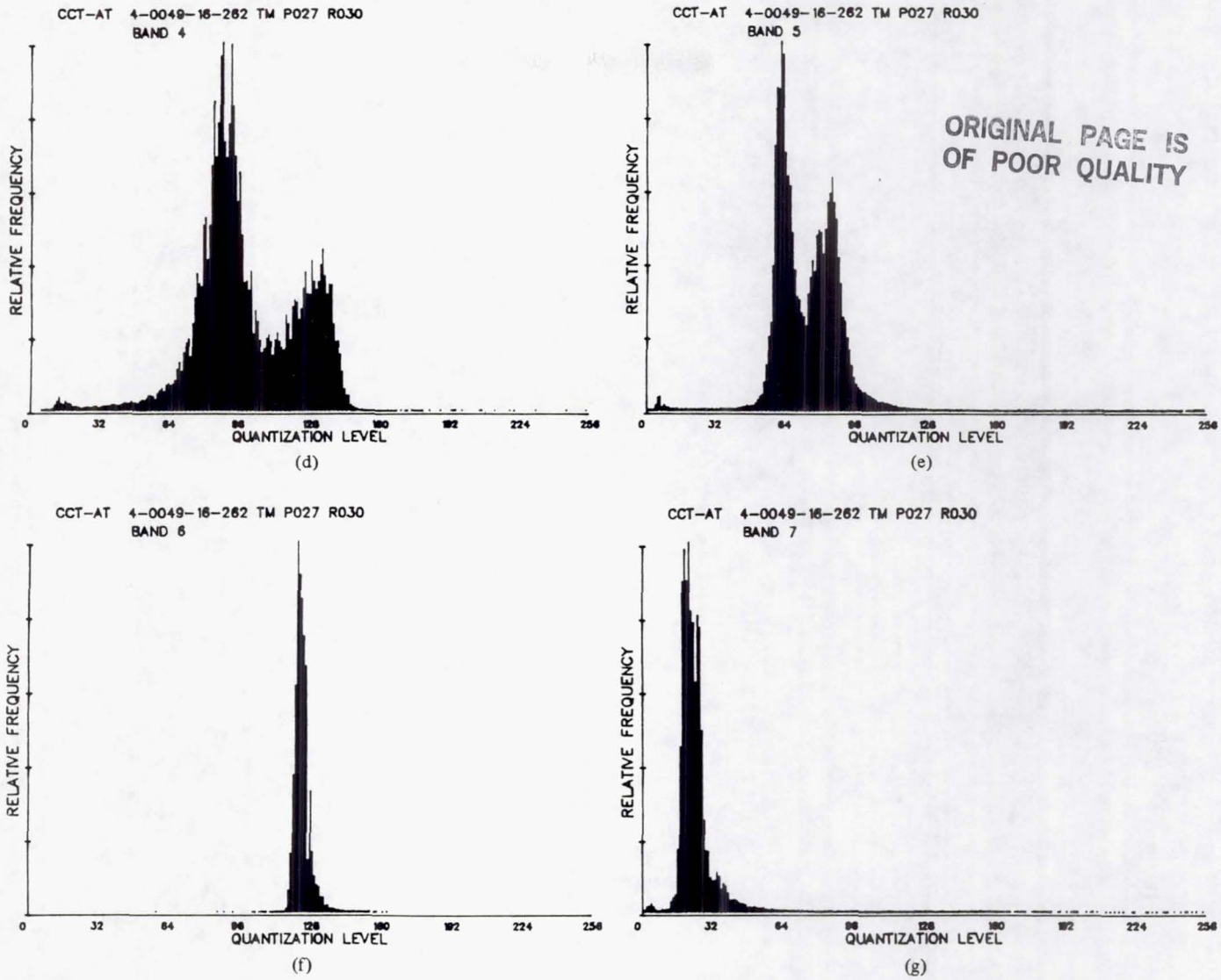

Fig. 7. Full-frame histograms for TM (Frame 40049-16262). (a) Band 1. (b) Band 2. (c) Band 3. (d) Band 4. (e) Band 5. (f) Band 6. (g) Band 7.

terize the scan-direction effect, the ratio of forward-scan signal level to reverse-scan signal level was computed as a function of scan angle (pixel number). We found that the droop had an exponential character and appeared to be proportional to the magnitude of the signal. This behavior is consistent with that of an ac coupled system with not quite complete dc restoration. To produce a preliminary model of the effect, it was convenient to fit the data to an exponential decay model. From these fits, we derived the following preliminary correction model.

$$S(p) = \frac{S_0(p)}{1 + A\,[\exp(-KM) - 1]}$$

where

$S_0(p)$ is the original signal for pixel "p".

$S(p)$ is the corrected signal value for pixel "p".

p is the pixel number, counting from West edge of scene.

p_f, p_r are the pixel offsets.

$M = (p_f + p)$ for forward scans = pixel number referenced to start of scan.

$(p_r - p)$ for reverse scans.

K is the time constant (reciprocal of the number of pixels of active scan required for 63 percent of the decay to occur).

A is the factor determining magnitude of total decay.

The model was fit with the constraint that A and K be identical for forward and reverse scans. The result of fitting this model to data from Band TM1 from the Iowa scene is illustrated in Fig. 12(a), and the predicted signal decay during forward and reverse scans is shown in Fig. 12(b). From this model, one can see that the decay begins prior to the first pixel, having decayed approximately 1 percent by that time. The total decay is approximately 2.25 percent by the end of the active scan. This results in the mean signal level of the forward scan being approximately 0.75 counts higher than the mean signal level of the reverse scan at the West edge of the scene, and approximately 0.75 counts lower at the East edge of the scene for Band TM1.

For this case (Band TM1, Scene 40049-16262), the p_f and p_r required for the fit resulted in the exponential decay beginning at the time of dc restore (different times for the two scan directions). During dc restore, a dark (no radiance) level

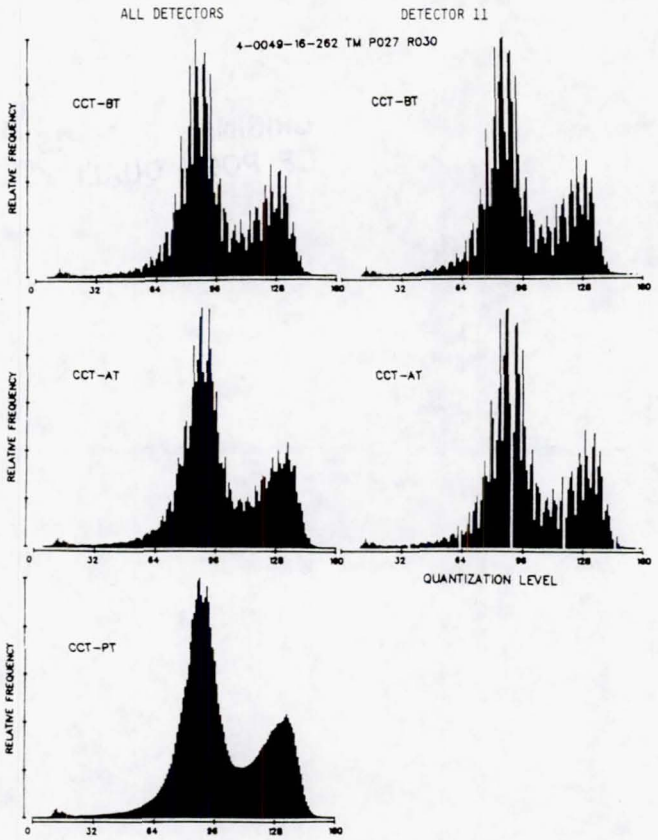

Fig. 8. Quantization-level histograms, Band TM4.

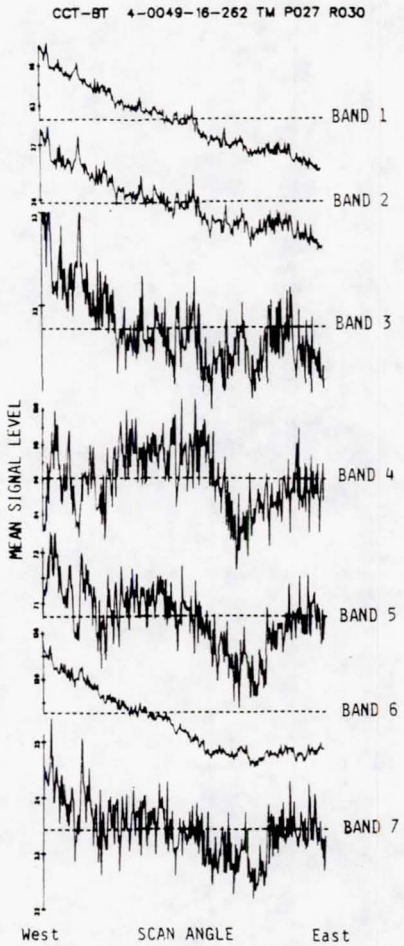

Fig. 9. TM scan-angle effect.

is presented to the detectors, and a dc level capacitor is charged to a value which results in approximately two signal counts. This charge was designed to be held for the entire scan, having a time constant on the order of minutes [21]. The empirically derived scan-direction effect model suggests that this charge may be decaying much faster (time constant of the order of 10 ms).

We plan to continue our investigation of this effect, refine the preliminary correction model, and extend the analysis to other bands.

C. Level-Shift Artifact and Recommended Correction Procedure

1) Description of Artifact: When down-track profiles (mean signal versus scan-line number) for individual detectors (every 16th line) from CCT-BT and CCT-AT data were examined, two patterns of level shifts were observed as one progressed down the frame. All detectors exhibited to some degree these step changes in mean signal across entire scan lines, although for most detectors the magnitude of the level shift was < 0.5 signal count. Also, it was found that these level shifts were correlated among detectors. Each detector exists in one of four noise states representing the combinations of the two forms or patterns of level shift and their respective phases.

Form #1 of the level-shift artifact is exemplified by the first band, as illustrated in Fig. 13. TM1 Detectors 4, 12, 10, and 8 show the greatest effect, with level shifts of 2.2, 1.8, 1.0, and 0.75 signal counts, respectively, occurring at random and usually having several to many scans at a given level before shifting to the other level. A very noise-free definition of this pattern was obtained through analysis of nighttime frames of data from the reflective-band detectors. More than 6000 pixels were averaged to obtain each scan-line average value shown in Fig. 14.

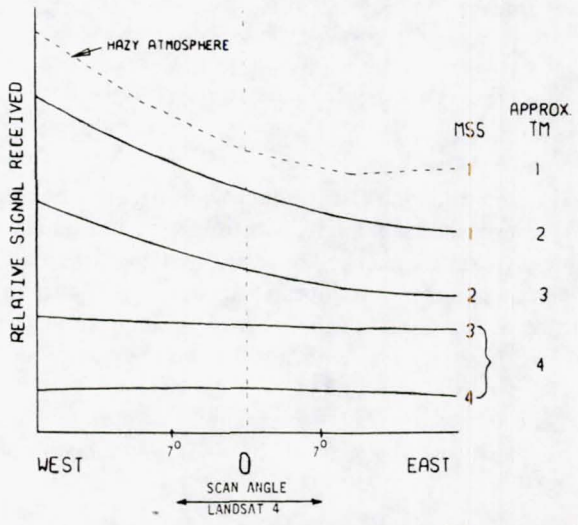

Fig. 10. Atmospheric scan-angle effects in MSS/TM Bands (Model results).

The pattern of the second form of level shifts is exemplified by Detector 7 of TM7, as shown in Fig. 15, again from night-

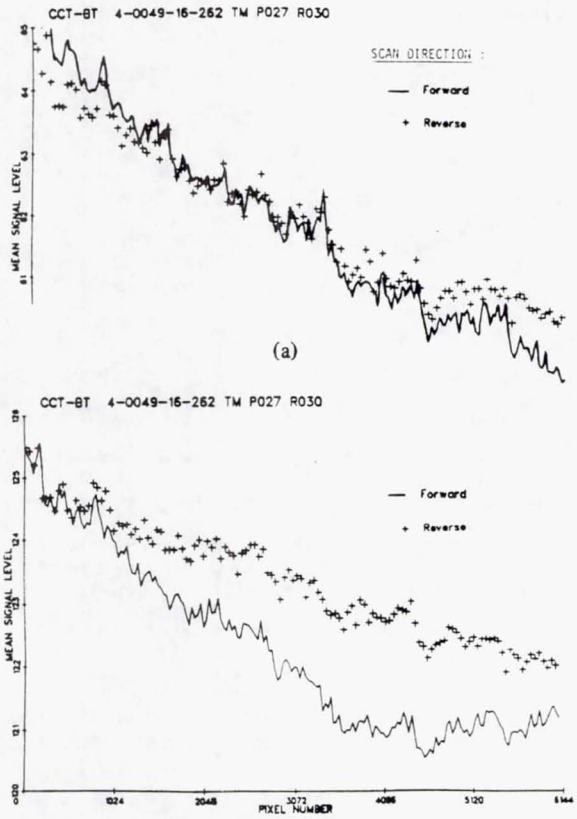

Fig. 11. TM scan-direction effect. (a) Band 1. (b) Band 6.

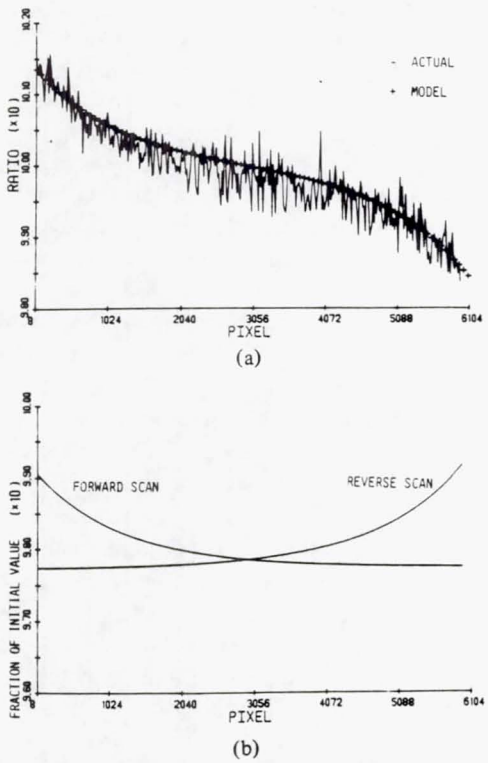

Fig. 12. Scan-direction artifact and model for Band TM1. (a) Ratio of mean forward-scan signal to mean reverse-scan signal. (b) Predicted decay of signal with time.

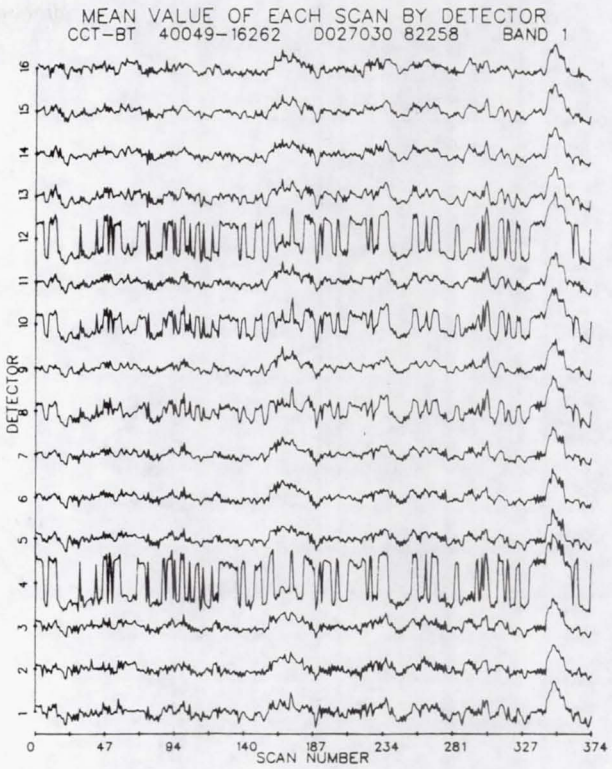

Fig. 13. Down-track profiles: Scan averages of scene data, before correction, band TM1.

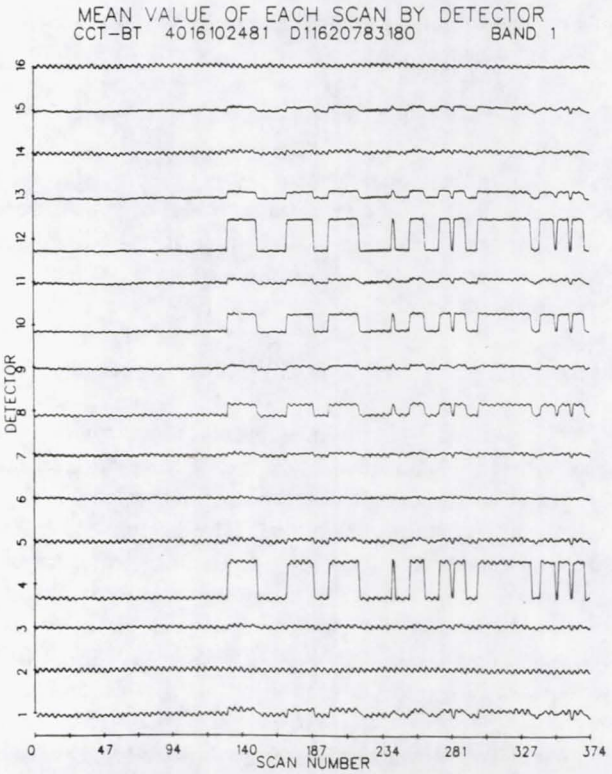

Fig. 14. Scan averages (by detector) of nighttime scene data, Band TM1.

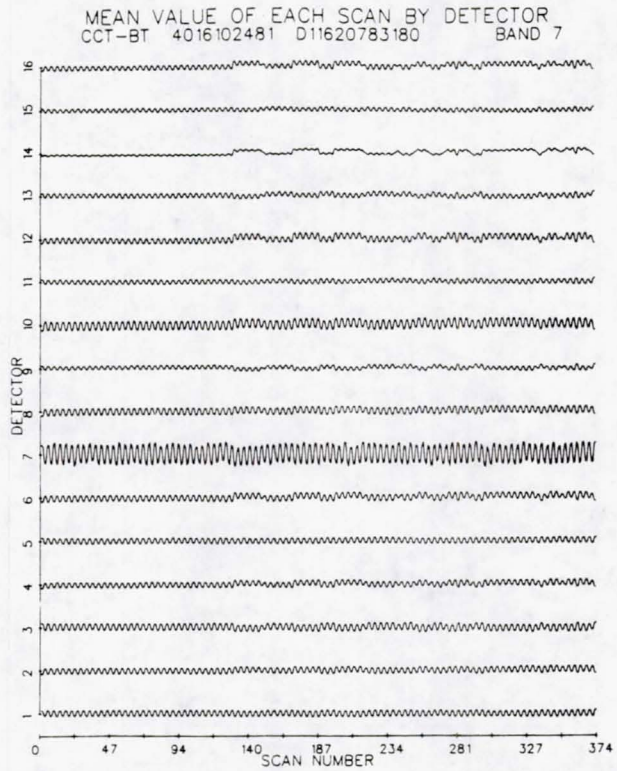

Fig. 15. Scan averages (by detector) of nighttime scene data, Band TM7.

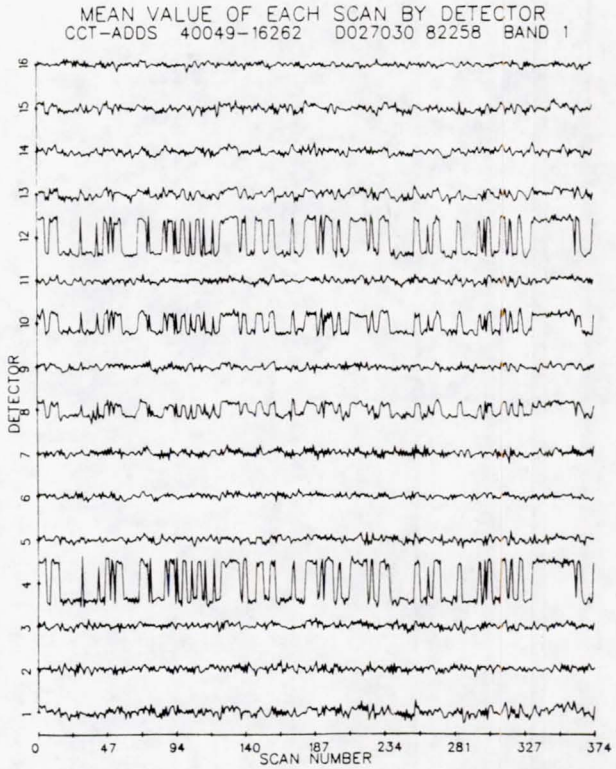

Fig. 16. Scan averages (by detector) of calibration shutter data, band TM1.

time data. This form #2 noise pattern is characterized by much more regular and frequent level shifts than form #1, often two mirror sweeps in each state.

While we have observed the form #2 level-shift noise patterns in all of the frames we have analyzed, the form #1 pattern was absent in the most recent scene we examined (Grand Bahamas) and a portion ($\sim\frac{1}{3}$) of the earlier Augusta night scene (Fig. 14). Nevertheless, level-shift artifacts have occurred sufficiently often to warrant development of a correction procedure. For example, level shifts of the magnitudes observed in TM1 could seriously interfere with quantitative applications of TM data, such as in bathymetry [22]. Although we have not identified the specific noise sources in the sensor, we believe we have characterized the level-shift artifacts sufficiently to develop empirical methods for substantially reducing their effects in scene data.

2) Recommended Correction Procedure: A correction procedure requires a diagnostic measure to determine the level-shift noise state of each detector on each scan line, in addition to a method for applying the corrections. Several alternatives for a diagnostic measure were examined. The most promising uses data values obtained when the calibration shutter is blocking the input radiation and no calibration lamps are in the field-of-view. We obtained several CCT-ADDS tapes from NASA/GSFC. These tapes contain the desired samples of dark calibration shutter data in two data windows, each 24 or 28 pixels in width. We averaged the samples in the window that followed the dc-restore procedure for each detector for each scan line. The resulting down-track profiles again reproduced the level-shift pattern observed in scene data. Upon comparing the calibration shutter profiles for TM1 (Fig. 16) with the corresponding profiles from scene data (Fig. 13) and nighttime data (Fig. 14), one can see that while they exhibit more random noise than the nighttime data ($\sim$25 samples averaged versus $>$6000), they do not exhibit the scene-dependent fluctuations evident in the scene data. In addition to serving as a diagnostic of the system noise state, the dark calibration shutter values also give an estimate of the level shift magnitudes.

Therefore, the correction procedure we recommend would compute the average of observations of the dark calibration shutter, after dc restore, and subtract the corresponding value from each pixel value on the scan line for the particular detector. Since this subtractive value will most likely be non-integer, incorporation of this offset would best be accomplished in the computation of the Radiometric Look-Up Table (RLUT), so as to eliminate an additional rounding/truncation step. This would, however, require an update of that table for each mirror sweep (every 16 scan lines). Even more frequent updates (e.g., for each pixel) would be desirable when correcting for the scan-angle effects discussed previously. However, this could impose severe implementation and operational problems.

An example of the potential effectiveness of this correction procedure is illustrated by a comparison of the down-track profiles of Figs. 13 and 17. The scene content is apparent in the TM1 data of Fig. 13, as is the effect of low-frequency noise. Fig. 17 is the result of subtracting the shutter data (Fig. 16) from the raw data (Fig. 13). Form #1 noise appears to be

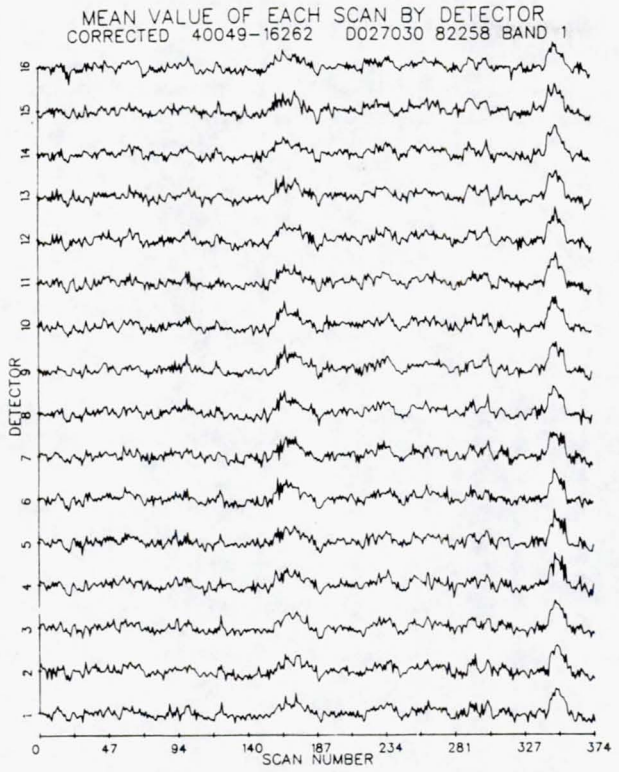

Fig. 17. Scan averages of scene data, after correction, Band TM1 (obtained by subtraction of calibration shutter averages).

eliminated, as have most differences among the down-track profiles of the detectors. In a similar comparison for TM7, form #2 noise was greatly reduced.

It has been recommended to NASA that this procedure be seriously considered for incorporation into the standard radiometric correction procedure for Landsat-4 TM data. Since the computation method used in this example was applied to the scan averages and therefore did not represent any added quantization effects that may result from a modified RLUT and pixel-by-pixel corrections, the recommended next step would be for NASA to analyze more recent data and, if warranted, implement a full correction procedure, test it on a trial basis on a number of scenes (including those we have analyzed) and carefully compare the new images and their statistics with those from the existing procedure.

VII. Summary

Engineering analyses of image data have been conducted for the Landsat-4 MSS and TM sensors. The image data were generally found to be of high quality and the TM gave evidence of several improvements over MSS, in its spatial and spectral characteristics.

The MSS analyses provided good evidence that Landsat-4 MSS data are of the same high quality as previous three Landsats, with comparable dynamic range and target responses, a good detector equalization procedure, and an accurate linear response to received radiance. Only two artifacts not noted in previous Landsats were found, and they were quantified. One is a geometric scan line length variation in Landsat "A" tapes, a variation that should not be a problem for the routine processing performed by the EROS Data Center to produce fully corrected "P" type data. The other artifact is a coherent noise effect in all bands, having an amplitude of less than one count. This noise causes a minor but distracting diagonal striping pattern on images of relatively uniform areas and would require substantial processing to be routinely removed or reduced. A well-defined linear relationship was determined to adjust Landsat-4 MSS signals so they follow a radiance response characteristic equivalent to that of Landsat-3. Based on less data, a simliar relationship was determined for Landsats-2 and -4.

Landsat-4 TM data were found to have very good spatial resolution and overall good radiometric data quality. Radiometric equalization of detectors was found to be close to the theoretical limit of quantization error, except for two relatively low-amplitude artifacts. The first was a scan-direction artifact caused by signal droop during the active portions of each forward and reverse scan. This artifact was most pronounced in TM1 of the reflective bands, while the thermal band (TM6) had a unique pattern. The second artifact was a low-frequency scan-related level shift which occurred in two forms, leading to four system noise states. Again, this artifact was most evident in TM1. Initial correction procedures have been developed and recommended for further evaluation. The presence of scan-angle effects due to atmosphere characteristics and scene bidirectional-reflectance effects was noted and it is suggested that attention be directed toward development of normalization procedures.

Upon comparing coincident MSS and TM data for one agricultural scene, high correlation values were found between MSS bands and the comparable TM bands. When spectral transforms were applied, Greenness variables for the two sensors were almost perfectly correlated. Their Brightness variables were less well correlated, likely due to contributions from TM bands covering regions not covered by MSS. Striking differences were observed in their ability to spatially resolve detail in this interesting agricultural scene.

Acknowledgment

The authors wish to acknowledge the contributions and support of R. Horvath and R. Cicone of ERIM in establishing and conducting this project.

References

[1] V. V. Salomonson and R. Koffler, "An overview of Landsat-4 status and results from Thematic Mapper data analysis," in *Proc. 17th Int. Symp. on Remote Sensing of Environ.*, ERIM, (Ann Arbor, MI), May 1983.

[2] J. L. Engle and O. Weinstein, "The Thematic Mapper–An overview," *IEEE Trans. Geosci. Remote Sensing*, vol. GE-21, no. 3, pp. 258–265, July 1983.

[3] E. P. Beyer, "Thematic Mapper geometric correction processing," in *Proc. 17th Int. Symp. on Remote Sensing of Environ.*, ERIM, (Ann Arbor, MI), May 1983.

[4] D. P. Rice and W. A. Malila, "Investigation of radiometric properties of Landsat-4 MSS," in *Proc. Landsat-4 Early Results Symp.*, NASA Goddard Space Flight Center, Greenbelt, MD, Feb. 1983.

[5] —, Final Report on Investigation of Radiometric Properties of the Landsat-4 Multispectral Scanner, ERIM Rep. no. 163200-3-F, Environmental Research Institute of Michigan, Ann Arbor, MI 48107, Aug. 1983.

[6] M. D. Metzler and W. A. Malila, "Scan-angle and detector effects

in Thematic Mapper radiometry," in *Proc. Landsat-4 Early Results Symp.*, NASA Goddard Space Flight Center, Greenbelt, MD, Feb. 1983.
[7] —, "Radiometric characterization of Thematic Mapper full-frame imager," in *Proc. SPSE/ASP Conf. on Techniques for Extraction of Information from Remotely Sensed Images*, (Rochester, NY), Aug. 1983.
[8] *Proc. Landsat-4 Early Results Symp.*, NASA Goddard Space Flight Center, Greenbelt, MD, Feb. 1983.
[9] R. C. Singleton, "On computing the fast fourier transform," *Comm. ACM*, vol. 10, no. 10, pp. 647-654, 1967.
[10] E. P. Crist, "Comparison of coincident Landsat-4 MSS and TM data over an agricultural region," in *Proc. ASP-ACSM Convention*, Mar. 1984.
[11] R. J. Kauth and G. S. Thomas, "The tasseled cap–A graphic description of the spectral-temporal development of agricultural crops as seen by Landsat," *Proc. Symp. on Machine Processing of Remotely Sensed Data*, Purdue University, West Lafayette, IN, pp. 4B41-4B51, 1976.
[12] E. P. Crist and R. C. Cicone, "A physically-based transformation of Thematic Mapper data–The TM tasseled cap," this issue, pp. 256-263.
[13] B. P. Clark and R. Dasgupta, "Landsat-4 Multispectral Scanner (MSS) subsystem radiometric characterization", W. Alford and J. Barker, Eds., NASA Goddard Space Flight Center, Greenbelt, MD, Feb. 1983.
[14] A. Oppenheim and R. Shafer. *Digital Signal Processing.* Englewood Cliffs, NJ: Prentice Hall, 1975.
[15] W. Likens, AMES Research Center, National Aeronautics and Space Administration, Moffet Field, CA, private communication, 1983.
[16] H. W. Warriner, U. S. Department of Commerce Memo E/SP4:HW, EROS Data Center, Sioux Falls, SD, Mar. 30, 1983.
[17] H. H. Kieffer, E. Eliason, P. Chavez, R. Batson, and W. Borgeson, "Thematic Mapper intraband radiometric performance," in *Proc. Landsat-4 Early Results Symp.*, NASA Goddard Space Flight Center, Feb. 1983.
[18] W. A. Malila and R. F. Nalepka, "Atmospheric effects in ERTS-1 data, and advanced information extraction techniques," in *Proc. Symp. on Significant Results Obtained from the Earth Resources Technology Satellite-1*, NASA Goddard Space Flight Center, pp. 1097-1104, 1973.
[19] W. A. Malila, J. M. Gleason and R. C. Cicone, "Atmospheric modeling related to Thematic Mapper scan geometry," Final Rep. NAS9-14819, NASA Johnson Space Center, 1976.
[20] J. V. Dave, "Extensive data sets of the diffuse radiation in realistic atmospheric models with aerosols and common absorbing gases," *Solar Energy*, vol. 21, pp. 361-369, 1978.
[21] J. Engle, Santa Barbara Research Center, Santa Barbara, CA, Private Communication, Jan. 29, 1983.
[22] D. R. Lyzenga, "Passive remote sensing techniques for mapping water depth and bottom features," *Appl. Opt.* vol. 17, no. 3, p. 379, 1978.
[23] J. L. Engle, J. C. Lansing, Jr., D. G. Brandshaft, and B. J. Marks, "Radiometric performance of the Thematic Mapper," in *Proc. the Landsat-4 Early Result Symp.*, Goddard Space Flight Center, Greenbelt, MD, Feb. 1983.

*

William A. Malila (S'55-M'57) was born in Kalamazoo, MI. He received B.S. and M.S. degrees in electrical engineering from Michigan State University, E. Lansing, MI, and Stanford University, Stanford, CA, in 1956 and 1960, respectively. His Ph.D. degree in forestry, with a remote sensing concentration, was received from the University of Michigan (U of M), Ann Arbor, MI in 1974.

Since joining the technical staff of the Willow Run Laboratories of the U of M (now the Environmental Research Institute of Michigan (ERIM)), Ann Arbor, MI, in 1960, he has been active in the development and testing of techniques for extracting information from remotely sensed data, especially multispectral scanner data, and the use of models and system analysis for better understanding phenonomenology and interactions. He has participated in technical research and management of NASA-sponsored supporting research activities for projects such as LACIE and AgRISTARS, and serves as Principal Investigator for the effort described in this paper.

*

Michael D. Metzler was born in Nappanee, IN. He received the B.S. and M.S. degrees in physics from Manchester College and Michigan State University, respectively.

Prior to joining the Environmental Research Institute of Michigan (ERIM) in 1980, he was employed as a Systems Programmer first by IBM's Federal Systems Division and then by Burroughs Corporation. In his four years at ERIM, he has been active in several areas of civilian remote sensing, ranging from development and implementation of agricultural remote sensing procedures to engineering analyses of sensor systems and thermal modeling.

*

Daniel P. Rice was born in Corvallis, OR in 1948. He received the B.S. and M.S. degrees in physics from the University of Michigan in 1970 and 1972, respectively.

Since 1972, he has been a Research Engineer with the Environmental Research Institute of Michigan, and has carried out work in the areas of reflectance modeling, agricultural crop acreage and yield estimation, software system design, and atmospheric effects correction.

*

Eric P. Crist received the B.S. degree in forestry from the University of Michigan, and carried out graduate studied related to remote detection of forest properties, also at the University of Michigan.

Since joining ERIM in 1977, as part of the Infrared and Optics Division, he has participated in research into the the use of satellite data for forestry and agricultural applications, particularly in the areas of information extraction and spectral features development.

APPENDIX B

Characterization and Comparison of Landsat -4 and Landsat -5 Thematic Mapper Data

Characterization and Comparison of Landsat-4 and Landsat-5 Thematic Mapper Data*

Michael D. Metzler and *William A. Malila*
Environmental Research Institute of Michigan, P.O. Box 8618,
Ann Arbor, MI 48107

ABSTRACT: Analyses of the characteristics of Landsat Thematic Mapper (TM) image data are described, and results are summarized. Emphasis is placed on radiometric characterization, development of response models, and on comparisons between data from Landsats 4 and 5. In general, the data quality was excellent; however, some anomalies were found. Three main topics are (a) systematic within-scan-line signal droop/rise, (b) random scan-correlated level shifts, and (c) radiometric (signal amplitude) relationships between Landsat-4 and Landsat-5. The systematic droop/rise effect was found in data from both Landsats 4 and 5. Daytime signals droop across the scan line while nighttime signals in the reflective bands rise across the scan line. The magnitude of the droop/rise appears to be a function of the signal magnitude and average value of the signal throughout a scan cycle. Scan-correlated level-shift noise also was observed in data from both sensors, but with different patterns. Low-amplitude, low-frequency coherent noise effects also were measured. The analysis of simultaneously acquired Landsat-4 and Landsat-5 TM data permitted a direct empirical comparison of the relative radiometric responses of their respective spectral bands. Relationships between their respective signal values were developed, and sensor dynamic range considerations are discussed. It was determined that multiplicative factors ranging from 0.987 to 1.145 were required to convert the signal counts from Landsat-4 TM spectral bands to corresponding Landsat-5 equivalent signals. Radiance values exhibited corresponding differences, pointing to residual errors in radiometric calibration. Low-level clipping was evident in the radiometrically corrected Landsat-5 bands 5 and 7 data. The temperature range covered by the full 8-bit data range of TIPS-processed TM band 6 data was found to be approximately 200°K to 340°K, not 260°K to 320°K as specified.

INTRODUCTION

SINCE THE LAUNCH of Landsat-4 in July 1982, numerous studies of the quality of Thematic Mapper (TM) image data have been performed under the auspices of the National Aeronautics and Space Administration's (NASA's) Landsat Image Data Quality Analysis (LIDQA) Program. As part of this program, we have performed engineering analyses of Thematic Mapper image data with our efforts concentrated on radiometric characterization of the sensor. In general, we have found the data quality to be excellent. However, anomalies do exist in the data from both Landsat-4 and Landsat-5 TM. The analyses of Landsat-4 TM image data were previously described in detail by the authors (Metzler and Malila, 1983b; Malila *et al.*, 1984; Metzler and Malila, 1983a) and are summarized below. This paper concentrates on recent analyses of Landsat-5 TM data and comparisons of the radiometry of the two sensors. Specific topics covered are (a) within-line droop, a phenomenon whereby the signal levels of the sensor change systematically during the active scan; (b) scan-correlated level shifts, an effect which raises or lowers the signal level of all pixels in a scan line or set of scan lines; and (c) comparison of Landsat-4 and Landsat-5 radiometric corrections. Other analyses of TM data anomalies may be found elsewhere in this issue (e.g., Kieffer *et al.*, 1985).

WITHIN-LINE DROOP

Earlier examination of Landsat-4 TM average scan lines indicated significant differences in the signals returned from the western edge of a scene compared to those observed at the eastern edge of the same scene. This effect was most apparent in the shortest wavelength spectral band (band 1), and was observed in all the spectral bands to some extent. A combination of bidirectional reflectance, atmospheric, and shadowing effects, as well as sun-view angle geometry can explain the effect observed. More careful examination of the average scan data, however, revealed a confounding effect due to dif-

* This research was sponsored by the U.S. National Aeronautics and Space Administration, Goddard Space Flight Center, Greenbelt, MD, under Contract NAS5-27346.

PHOTOGRAMMETRIC ENGINEERING AND REMOTE SENSING,
Vol. 51, No. 9, September 1985, pp. 1315-1330.

0099-1112/85/5109-1315$02.25/0

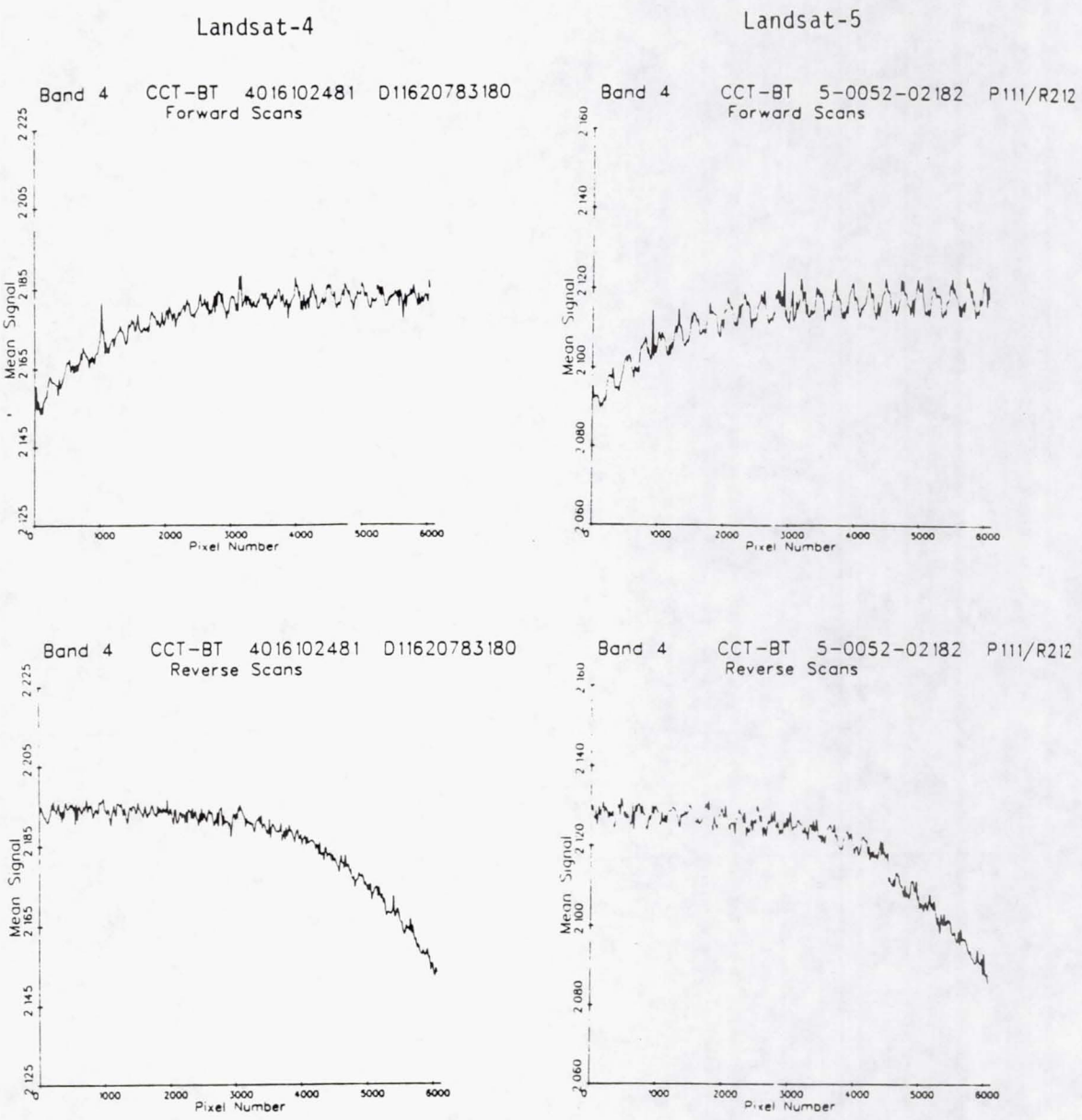

FIG. 1. Landsat-4 and Landsat-5 TM nighttime within-scan rise effect—band 1.

ferent sensor response characteristics related to the direction of scan in bands 1 through 4. The scan-direction difference took the form of a droop in signal with time during active scan, which appeared as a signal decrease with increasing pixel number for forward scans, and a signal increase with increasing pixel number for reverse scans. This effect was found in nighttime reflective-band data as well, but taking the form of a signal rise with time instead of a droop.

SCAN-CORRELATED LEVEL SHIFTS

In Landsat-4 TM data, an effect was analyzed which changed the signal of all samples within a scan-line or group of scan-lines by up to 2.0 video quantum levels (DN). The changes were aperiodic, occurring at random intervals with the level shifting during mirror turn-around time. All affected detectors shifted levels at the same time, with the level shifts following one of two patterns (most detectors

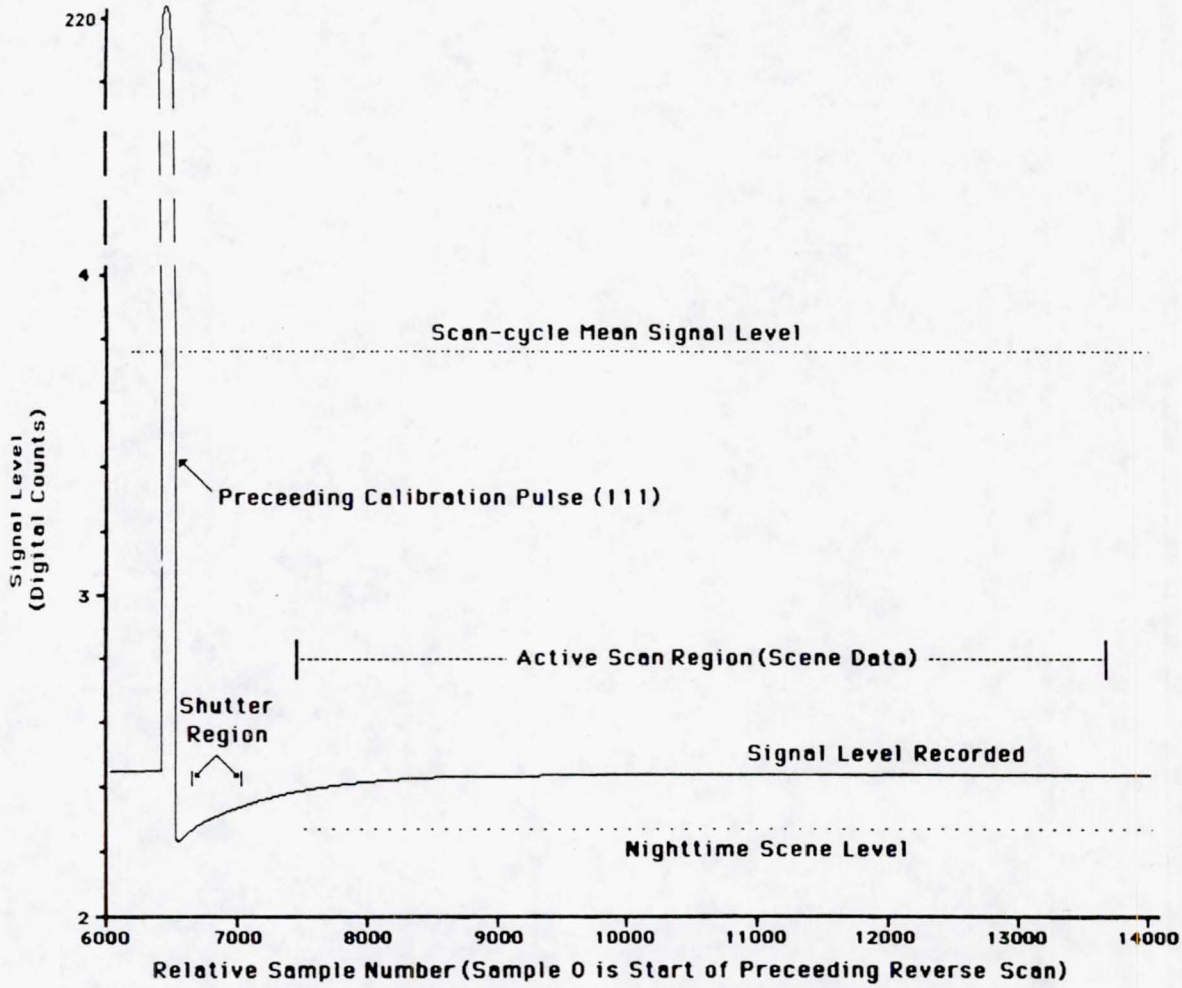

FIG. 2. Example nighttime reverse scan signal levels—band 1.

exhibited both patterns, but one was dominant). One pattern was exemplified by band 1 detector 4 with a peak-to-peak amplitude of 2.0 DN, the other by band 7 detector 7. These two patterns were labeled 'form #1' and 'form #2', respectively (later labeled 'type 4-1' and 'type 4-7', respectively, by Barker (1984)).

METHODS

All analyses to characterize the radiometry of the sensors were performed on digital computer compatible tape (CCT) data. Several types of CCT data were used, representing various stages of ground processing as well as calibration data. The analyses described in this paper generally were performed on full-frame TM image data, both to characterize full-frame effects and to take advantage of the large data volume (approximately 37 million pixels per band per frame) to improve the quality of the statistics generated.

Two primary methods were used to average the full-frame image data. In one case, to examine scan-angle effects, average scan lines were computed by averaging the columns of pixels down the entire frame. To analyze scan-direction effects, these average scan lines were stratified by scan direction, with the forward and reverse scan data being treated separately. The other type of averaging involved computing down-track profiles by averaging the rows of pixels across the entire frame, thereby computing an average signal value for each scan line. Each of these analyses was performed separately for each band and each detector of the sensors.

Earlier investigations by the authors (Malila *et al.*, 1984) demonstrated the value of using reflective-band (bands 1–5 and 7) TM data collected at

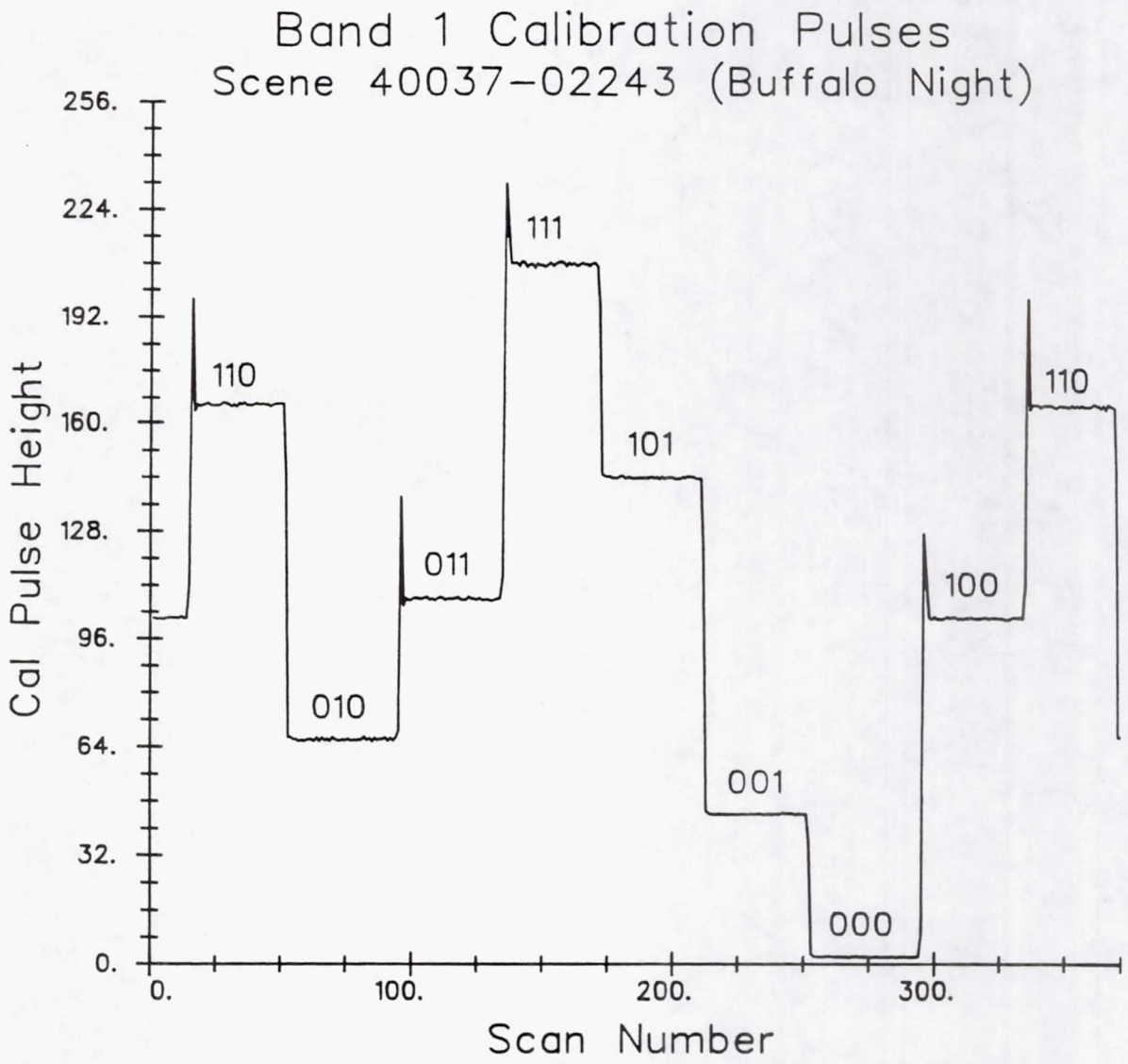

FIG. 3. Calibration lamp sequencing for band 1.

night for analysis of sensor data anomalies. The sensor sensitivities are such that no scene radiance is recorded, so any variations in the data are due to sensor noise effects. We again made extensive use of nighttime data in the analyses described herein, processing the data using the techniques described above.

Two techniques were employed to compare the radiometry of the Thematic Mappers on Landsat-4 and on Landsat-5, using a special data set which was collected simultaneously with both sensors. The first technique involved selecting a subimage of 3,564,000 pixels (1980 lines by 1800 pixels) from the Landsat-5 image and spatially registering it to the Landsat-4 TM image data. This registration was performed to subpixel accuracy using 50 control points and nearest neighbor resampling. The data in each subimage were averaged using 5 × 5 pixel cells to reduce any misregistration effects and to reduce the data volume while still retaining the data diversity. Linear regressions were performed with data from the two averaged images. Multiplicative and additive factors were computed for each band which can be used to relate the signals from one sensor to those expected from the other sensor for the same input radiance.

For the second comparison, histograms were computed for the subimages described above, and

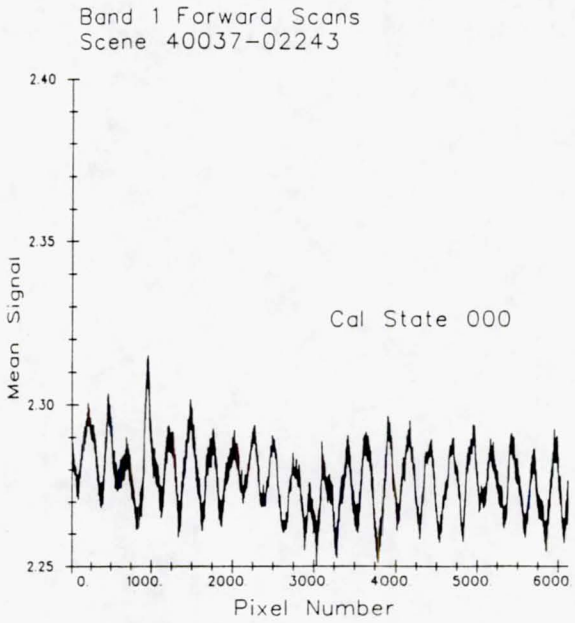

FIG. 4a. Nighttime forward scan signal rise for scans preceeded by calibration lamp state 000.

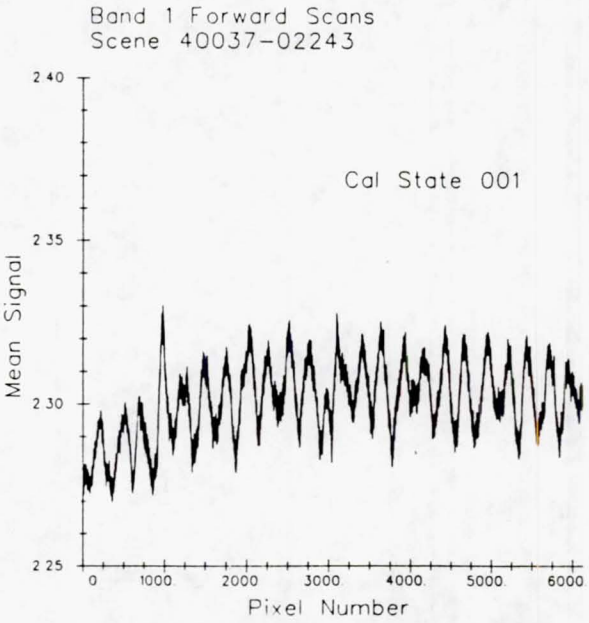

FIG. 4b. Nighttime forward scan signal rise for scans preceeded by calibration lamp state 001.

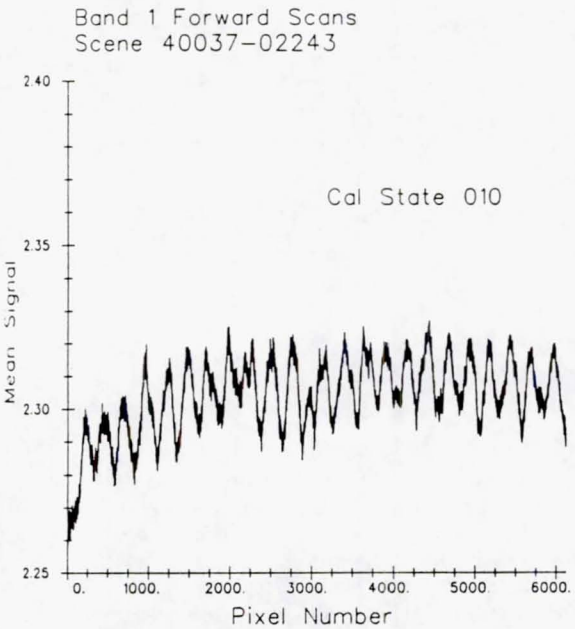

FIG. 4c. Nighttime forward scan signal rise for scans preceeded by calibration lamp state 010.

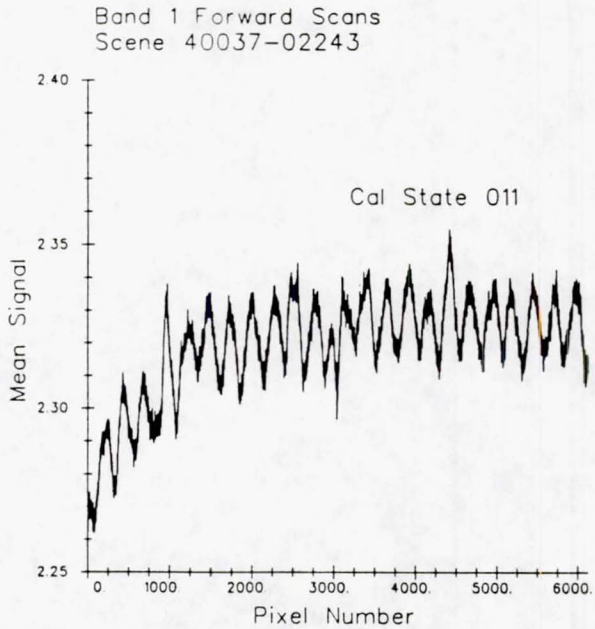

FIG. 4d. Nighttime forward scan signal rise for scans preceeded by calibration lamp state 011.

a histogram matching technique was employed to compute multiplicative and additive coefficients for relating data from one sensor to that of the other. Unlike the histogram matching procedure used in TM ground processing which equalizes means and standard deviations (Barker *et al.*, 1983), a procedure based on matching the cumulative distribution functions of the two data sets was employed. This technique is believed to have some advantages in making better use of the full range and distribution

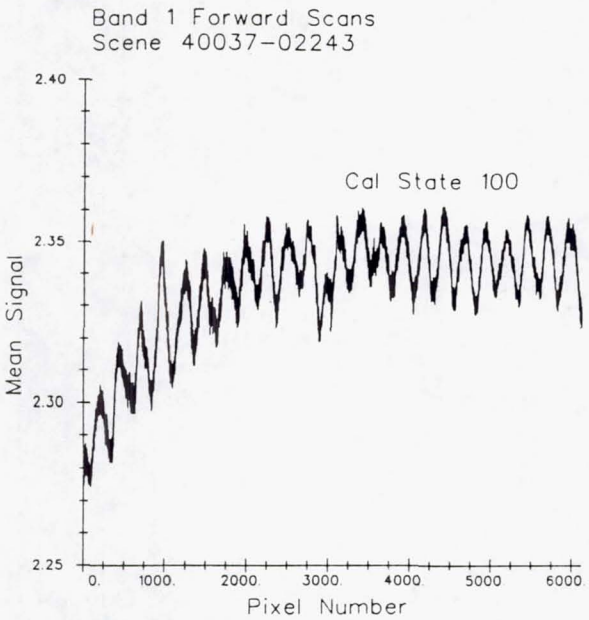

FIG. 4e. Nighttime forward scan signal rise for scans preceeded by calibration lamp state 100.

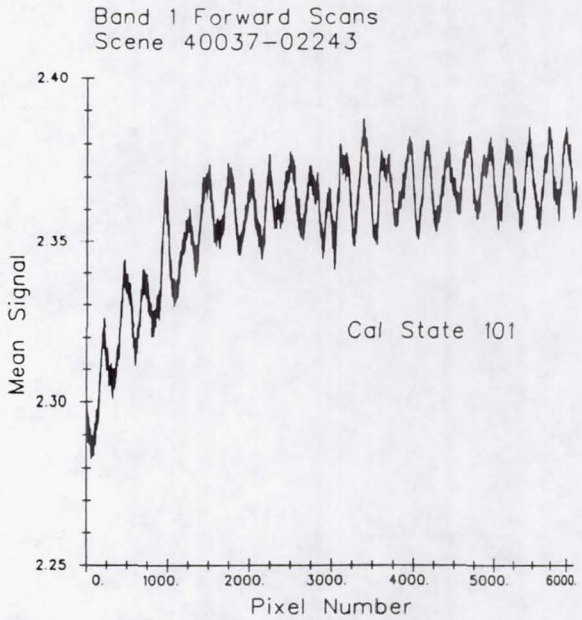

FIG. 4f. Nighttime forward scan signal rise for scans preceeded by calibration lamp state 101.

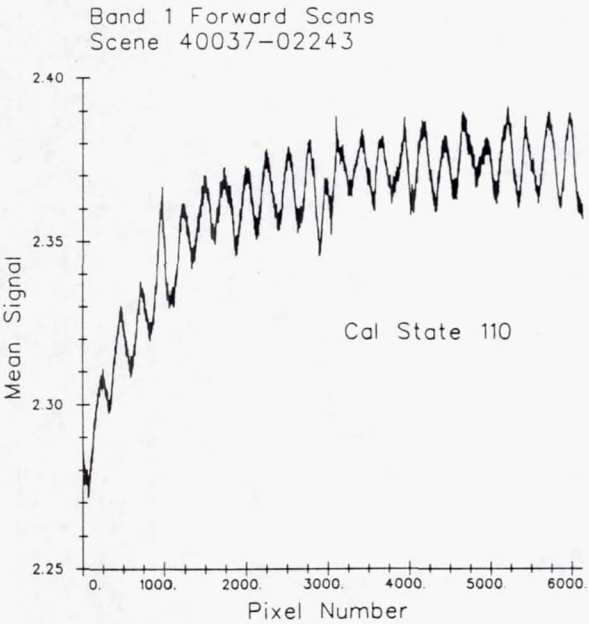

FIG. 4g. Nighttime forward scan signal rise for scans preceeded by calibration lamp state 110.

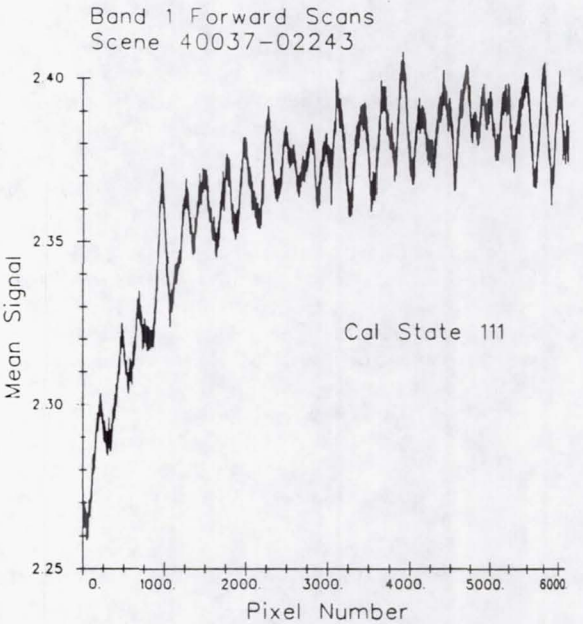

FIG. 4h. Nighttime forward scan signal rise for scans preceeded by calibration lamp state 111.

of data values in the histogram. Additionally, the histogram matching approach has much less stringent registration requirements than pixel or region matching approaches. For a region with a very small perimeter/area ratio, effects of slight misregistration would be minimal. The cumulative distribution function gives percentage of observations having signal values less than or equal to the designated

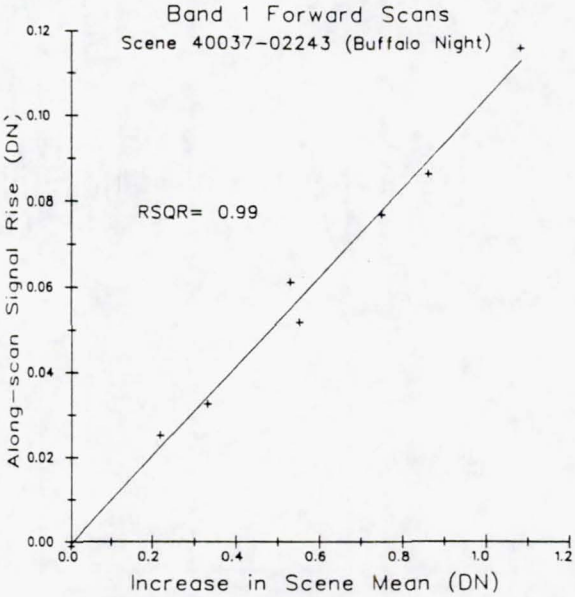

FIG. 5. Relationship of magnitude of signal rise and difference between scan-cycle mean and scene mean.

signal value. Interpolations were made to obtain the signal values corresponding to integer percentage values. Excluding end points, a regression of the corresponding percentile signal levels from the two sensors provided the desired correction coefficients.

RESULTS

Within-Line Droop

The single nighttime Landsat-5 TM scene (ID 5-0052-02182, Harrisburg, PA) available to us was used to quantify the within-scan droop/rise effect in Landsat-5 TM data. The average nighttime scan lines for band 4 of Landsat-5 TM are illustrated in Figure 1, along with data from Landsat-4 TM for comparison. Both forward and reverse scans are shown. The y-axes all have the same scale, i.e., 0.1 DN full scale, to facilitate comparison between sensors. Note that for reverse scans, pixel position 6000 is sampled prior to pixel position 1. Therefore, the effect is seen to be a signal rise with increasing time for both forward and reverse scans. In general, the within-scan rise has the same magnitude and time constant for the same band in each sensor. Magnitudes are greater in daytime data and the signals droop with increasing time, as will be discussed later.

Band 1 displays the greatest effect, with the mean reverse-scan signal increasing approximately 0.1 DN during the active scan. A simplified exponential decay model was fitted to the data for each of bands 1 through 4. For these bands, the time constant (time for magnitude of effect to decay to 1/e of original value) which produced the best fit ranged from 900 to 1100 pixel sample times, (approximately 9–10 milliseconds) for both Landsat-4 and Landsat-5 TM.

The mathematical model used is expressed by the equation:

$$S(p) = S_0 + Be^{-p/T} \quad (1)$$

Where:

$S(p)$ = signal returned by sensor for pixel p
S_0 = signal for p equal to infinity
B = magnitude of total droop/rise
T = time (pixels) required for signal to change by 63% of B
p = pixel number, with count starting with first image pixel (west-most for forward scans, east-most for reverse daytime scans).

Since the magnitude and time constant of the nighttime within-scan rise are essentially identical for Landsat-4 and Landsat-5, we would expect the daytime droop effects to be similar also. During daytime data acquisition when signal levels were much higher, we observed in Landsat-4 TM data a corresponding increase in the magnitude of the droop effect. In a daytime band 1 scene (ID 4-0049-16262) which had a scene mean of 61.9 DN, the magnitude of the droop was observed to be approximately minus 1.5 DN, with a time constant equivalent to approximately 900 pixels. At night, the magnitude of the rise was <0.15 DN, still with a time constant of 900 pixels for band 1. The mean scene level at night was 2.3 DN. Although qualitatively the daytime Landsat-5 effect appears similar to the daytime Landsat-4 effect, quantification of this effect in daytime Landsat-5 TM data awaits analysis of an appropriate scene in which variations in scene radiance have a relatively uniform spatial distribution.

The droop/rise effect was analyzed further to establish a hypothesis for its cause and a model for its description and potential use in correction. While the magnitude of the effect does not appear to be strictly proportional to the scene mean, it does appear as if the droop or rise is a drift toward the scan-cycle mean signal of the scene which also includes the signal values produced during shutter obscuration, calibration pulse, and DC restoration. This scan-cycle mean would be lower than the scene mean during the daytime due to the addition of the data acquired during shutter obscuration, and would be greater than the scene mean during nighttime data acquisition, where the scene itself is effectively a continuation of the shutter obscuration, and the calibration pulses drive the scan-cycle mean to a level slightly higher than the scene mean (see Figure 2). The hypothesis is that a-c coupling exists between the detector output and the analog-to-dig-

TABLE 1. MAGNITUDE AND PHASE OF LEVEL-SHIFT NOISE IN LANDSAT-4 SCENE 4-0161-02481

		Amplitude*		Separation of States (#S.D.)				Amplitude*		Separation of States (#S.D.)	
Band	Det	Form 1	Form 2	Form 1	Form 2	Band	Det	Form 1	Form 2	Form 1	Form 2
1	1	0.261	−0.162	3.1	1.9	4	1	0.256	0.047	6.6	1.2
1	2	−0.024	−0.188	.3	2.5	4	2	0.117	−0.084	3.3	1.9
1	3	0.077	−0.117	1.1	1.7	4	3	0.197	−0.031	2.3	.4
1	4	1.880	0.116	26.2	1.6	4	4	0.052	−0.072	1.3	1.8
1	5	0.120	−0.141	2.1	2.4	4	5	0.119	−0.013	3.7	.4
1	6	0.038	−0.060	.5	.8	4	6	0.316	−0.063	5.2	1.0
1	7	0.098	−0.077	1.6	1.2	4	7	0.073	−0.017	3.1	.7
1	8	0.569	−0.092	8.0	1.3	4	8	0.003	0.083	.1	2.4
1	9	0.146	0.043	2.0	.6	4	9	0.064	−0.023	1.9	.7
1	10	0.877	−0.053	13.2	.8	4	10	0.147	−0.013	5.0	.4
1	11	0.173	−0.063	2.1	.8	4	11	0.101	−0.017	4.0	.6
1	12	1.601	−0.011	24.3	.2	4	12	0.252	0.019	7.0	.5
1	13	0.313	−0.029	3.8	.3	4	13	0.063	0.008	1.5	.6
1	14	0.084	−0.124	1.2	1.8	4	14	0.087	−0.020	3.2	.7
1	15	0.171	−0.041	1.8	.4	4	15	0.114	−0.015	5.2	.6
1	16	−0.025	−0.123	.3	1.6	4	16	0.371	0.029	9.7	.7
2	1	0.246	−0.323	4.0	5.2	5	1	−0.018	0.060	.6	2.2
2	2	0.149	0.056	3.0	1.1	5	2	0.136	−0.103	3.6	2.8
2	3	−0.082	−0.202	1.2	3.0	5	3	−0.125	−0.067	4.6	2.5
2	4	0.203	0.027	5.0	.7	5	4	0.113	−0.038	3.3	1.1
2	5	0.072	−0.138	1.4	2.7	5	5	−0.183	−0.043	6.6	1.5
2	6	0.075	0.056	1.4	1.1	5	6	0.046	−0.085	1.1	2.6
2	7	0.004	−0.086	.1	2.0	5	7	0.017	0.143	.5	4.8
2	8	0.106	0.062	1.8	1.1	5	8	0.074	−0.200	2.6	6.9
2	9	0.039	−0.053	1.3	1.8	5	9	−0.085	0.023	2.7	.7
2	10	0.033	0.031	1.3	1.2	5	10	−0.086	0.744	2.7	22.7
2	11	0.056	−0.061	1.4	1.5	5	11	−0.022	0.046	.9	1.9
2	12	0.143	0.035	3.7	.9	5	12	0.006	0.061	.3	2.6
2	13	0.084	−0.101	1.7	2.1	5	13	−0.083	0.004	3.4	.2
2	14	0.064	0.043	1.7	1.2	5	14	−0.079	−0.082	3.8	3.9
2	15	0.097	−0.099	2.5	2.6	5	15	−0.211	−0.119	8.3	4.6
2	16	0.074	0.127	1.8	3.1	5	16	−0.017	−0.100	.7	4.3
3	1	0.484	−0.494	7.3	7.5	7	1	−0.034	0.302	1.3	11.5
3	2	0.296	0.273	7.3	6.7	7	2	0.054	−0.293	1.8	9.7
3	3	0.235	−0.275	4.9	5.3	7	3	−0.090	0.342	3.1	11.8
3	4	0.022	0.032	.7	.9	7	4	0.093	−0.273	3.4	9.9
3	5	0.304	−0.205	6.0	4.0	7	5	0.006	0.281	.2	10.8
3	6	0.248	0.086	5.7	2.0	7	6	0.123	0.308	1.3	10.4
3	7	0.155	−0.203	3.6	4.8	7	7	−0.040	0.960	.3	6.4
3	8	−0.088	−0.034	2.1	.8	7	8	0.066	−0.345	2.6	13.5
3	9	−0.051	−0.063	1.2	1.4	7	9	−0.109	0.197	4.2	7.5
3	10	0.253	0.055	4.0	.9	7	10	0.095	−0.461	3.3	15.1
3	11	0.003	−0.134	.2	4.0	7	11	−0.045	0.232	1.6	8.3
3	12	0.102	0.230	1.9	4.2	7	12	0.168	−0.297	5.3	9.1
3	13	0.215	−0.151	5.6	3.9	7	13	−0.087	0.224	2.8	7.1
3	14	0.209	0.180	4.2	3.6	7	14	0.198	−0.085	6.6	2.8
3	15	0.278	−0.262	6.9	6.5	7	15	−0.043	0.193	1.7	7.7
3	16	0.446	0.782	6.9	12.1	7	16	0.169	−0.253	5.5	8.2

* Negative amplitudes indicate level shifts with phase shifts of 180 relative to B1D4 (Form 1) or B7D7 (Form 2)

ital converter, producing a signal decay proportional to the departure from the scan-cycle mean.

To test this hypothesis, a scene of nighttime Landsat-4 TM data (scene 4-0037-02243) was segmented based on the calibration lamp state observed by the sensors prior to each scan. As illustrated in Figure 3, the internal calibration lamps sequence through the eight possible states, re-

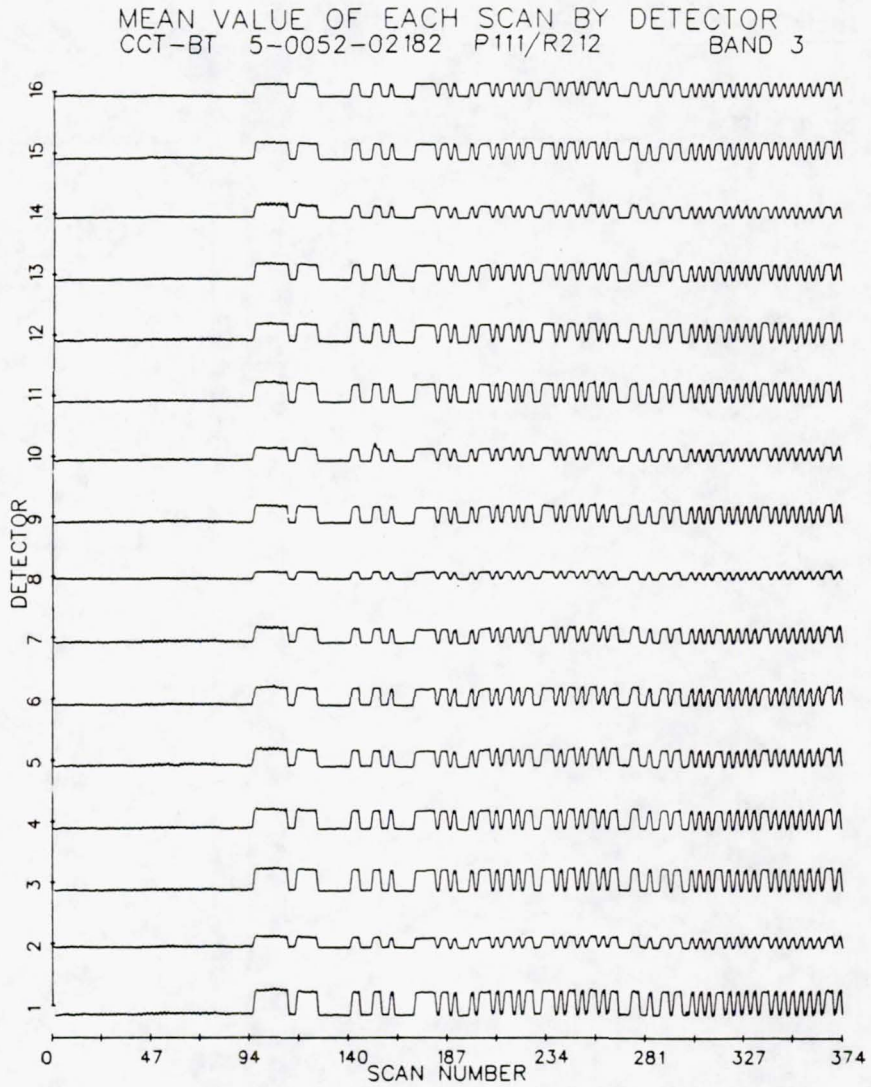

FIG. 6. Level shifts for Landsat-5 TM band 3 nighttime data.

maining in each state for approximately 40 scans (20 forward/reverse scan cycles). During nighttime reflective-band data collection, the signal pulses resulting from viewing these calibration lamps at the end of each scan are the only signals available to shift the scan-cycle mean from the scene mean. All scans with lamp state 000 (no lamps on) were grouped into one subimage, and seven other subimages were created for the other seven lamp states (001, 010, 011, 100, 101, 110, and 111, where each binary digit represents the state of one of the three calibration lamps). Average scan-lines were computed for each of these subimages, then smoothed and displayed as plots of mean signal level versus pixel position (see Figures 4a–4h). Qualitatively one can see that the effect is greatest when the calibration pulse adds the most to the scan-cycle mean (state 111, all lamps on), and is nonexistent in the case of no calibration pulse (scan-cycle mean equal to scene mean).

Quantitative support for the hypothesis of drift toward a scan-cycle mean was derived from data on the calibration tape (CCT-ADDS) associated with the image data. From the CCT-ADDS, the magnitude of the calibration pulse for each scan line could be computed, which in turn allowed calculation of the scan-cycle mean for each scan. The rise for each scan was computed and plotted against the difference between scan-cycle mean and scene mean as illustrated in Figure 5. Regression analysis indicated

TABLE 2. MAGNITUDE AND PHASE OF LEVEL-SHIFT NOISE IN LANDSAT-5 SCENE 5-0052-02182

Band	Det	Amplitude*	Separation of States (Number of Std. Dev.)	Band	Det	Amplitude*	Separation of States (Number of Std. Dev.)
1	1	0.036	0.9	4	1	0.285	11.0
1	2	−0.229	6.4	4	2	0.150	5.5
1	3	0.061	1.7	4	3	0.149	5.0
1	4	−0.184	4.2	4	4	0.205	8.4
1	5	0.044	1.3	4	5	0.044	3.3
1	6	−0.249	6.3	4	6	0.045	2.5
1	7	0.113	3.4	4	7	0.025	3.1
1	8	−0.208	5.2	4	8	0.016	0.6
1	9	0.042	1.3	4	9	0.078	2.8
1	10	−0.303	9.3	4	10	0.004	0.3
1	11	0.068	2.3	4	11	0.106	3.8
1	12	−0.216	5.4	4	12	0.016	0.7
1	13	−0.010	0.3	4	13	0.138	4.4
1	14	−0.307	8.5	4	14	0.081	2.2
1	15	0.001	0.0	4	15	0.085	3.0
1	16	−0.266	7.6	4	16	0.015	0.5
2	1	0.523	16.3	5	1	0.135	6.8
2	2	0.084	4.6	5	2	0.006	0.4
2	3	0.239	11.5	5	3	0.190	13.6
2	4	−0.009	1.1	5	4	−0.023	1.7
2	5	0.178	10.5	5	5	−0.067	4.5
2	6	0.070	7.2	5	6	−0.128	9.3
2	7	0.157	8.7	5	7	0.008	0.6
2	8	0.065	7.3	5	8	−0.115	9.0
2	9	0.079	8.2	5	9	0.056	4.3
2	10	0.012	2.4	5	10	0.019	0.5
2	11	0.086	6.9	5	11	0.100	7.4
2	12	0.016	2.3	5	12	−0.129	6.9
2	13	0.177	9.5	5	13	0.022	1.7
2	14	0.075	8.4	5	14	−0.074	5.0
2	15	0.159	10.1	5	15	−0.088	7.4
2	16	0.263	12.6	5	16	−0.137	9.7
3	1	0.470	14.1	7	1	0.019	1.1
3	2	0.196	8.1	7	2	−0.013	0.8
3	3	0.437	14.3	7	3	−0.050	3.1
3	4	0.389	13.9	7	4	−0.110	6.8
3	5	0.317	8.2	7	5	0.001	0.1
3	6	0.340	12.0	7	6	−0.095	6.6
3	7	0.286	7.8	7	7	0.146	8.9
3	8	0.141	8.5	7	8	0.159	10.2
3	9	0.326	10.5	7	9	0.161	11.7
3	10	0.250	9.4	7	10	−0.156	9.4
3	11	0.371	12.9	7	11	0.107	7.0
3	12	0.351	11.8	7	12	−0.060	4.1
3	13	0.318	12.8	7	13	0.032	2.3
3	14	0.237	7.7	7	14	0.038	2.1
3	15	0.321	12.6	7	15	0.022	1.6
3	16	0.257	11.8	7	16	−0.116	8.0

* Negative amplitudes indicate level shifts with phase shifts of 180 relative to band 3 detectors.

an excellent fit (R^2 of 0.99), which strongly supports the hypothesis, indicating that the parameter B in the model expressed above is a function of the difference between the scan-cycle mean and the scene mean. Although this analysis was performed only for forward scans of band 1 of one Landsat-4 TM image, experience to date indicates that the result may be extended to both scan directions of bands 1 through 4 of both Landsat-4 and Landsat-5 Thematic Mappers with a high degree of confidence.

This droop/rise effect has been observed for the primary focal plane bands only. For both Landsats, bands 5 and 7 show essentially no change in mean signal level within the scan line, with perhaps a

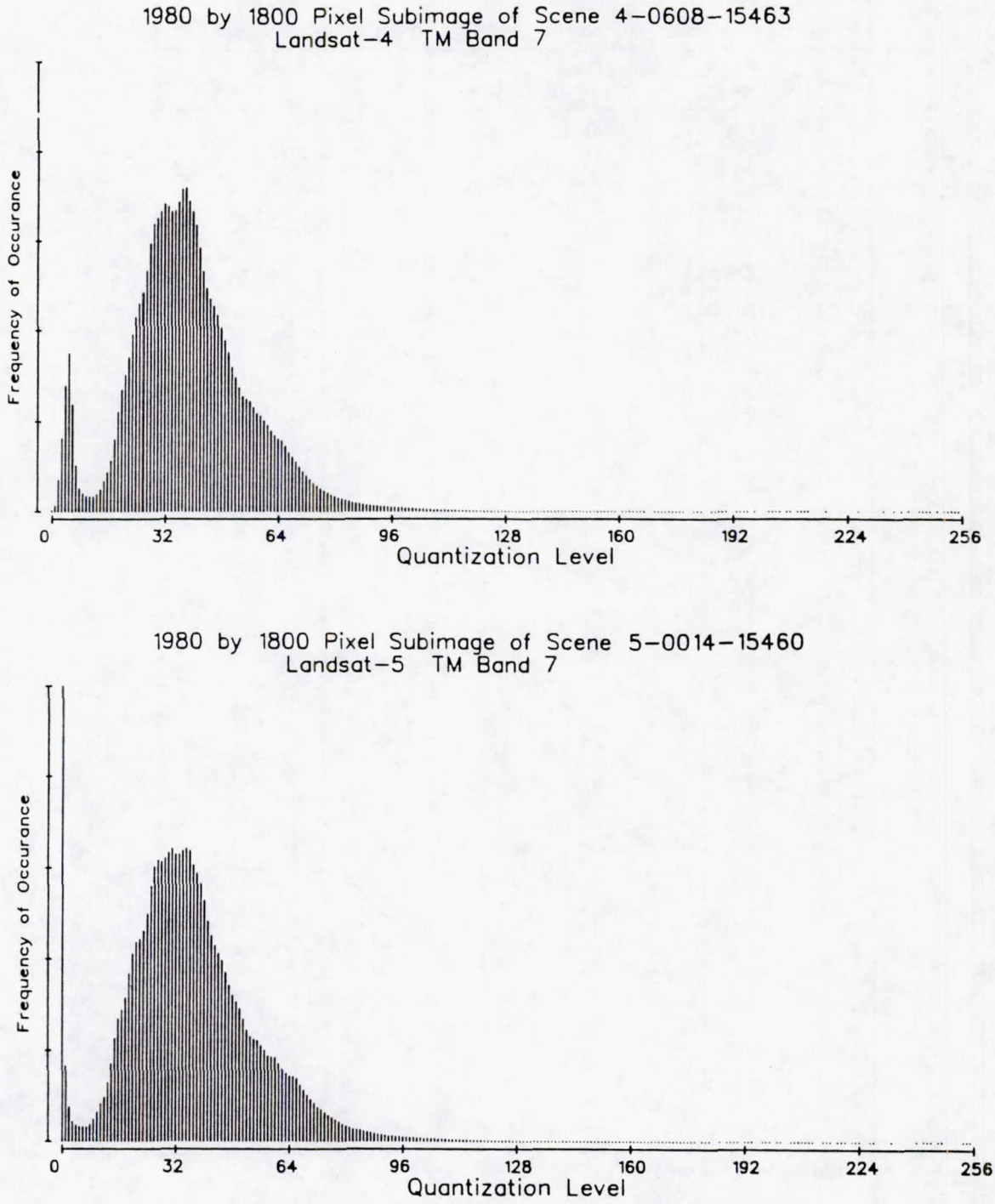

FIG. 7. Landsat-4 and Landsat-5 TM band 7 histograms for coincident regions.

slight change in the *opposite* direction to that seen in bands 1 through 4. Band 6 mean signal levels have been observed to change within scan lines in a variety of patterns. Detailed analysis of potential within-scan effects in band 6 is made more difficult by the absence of any constant scene data comparable to the nighttime data in the reflective bands. Even a completely uniform ground scene would

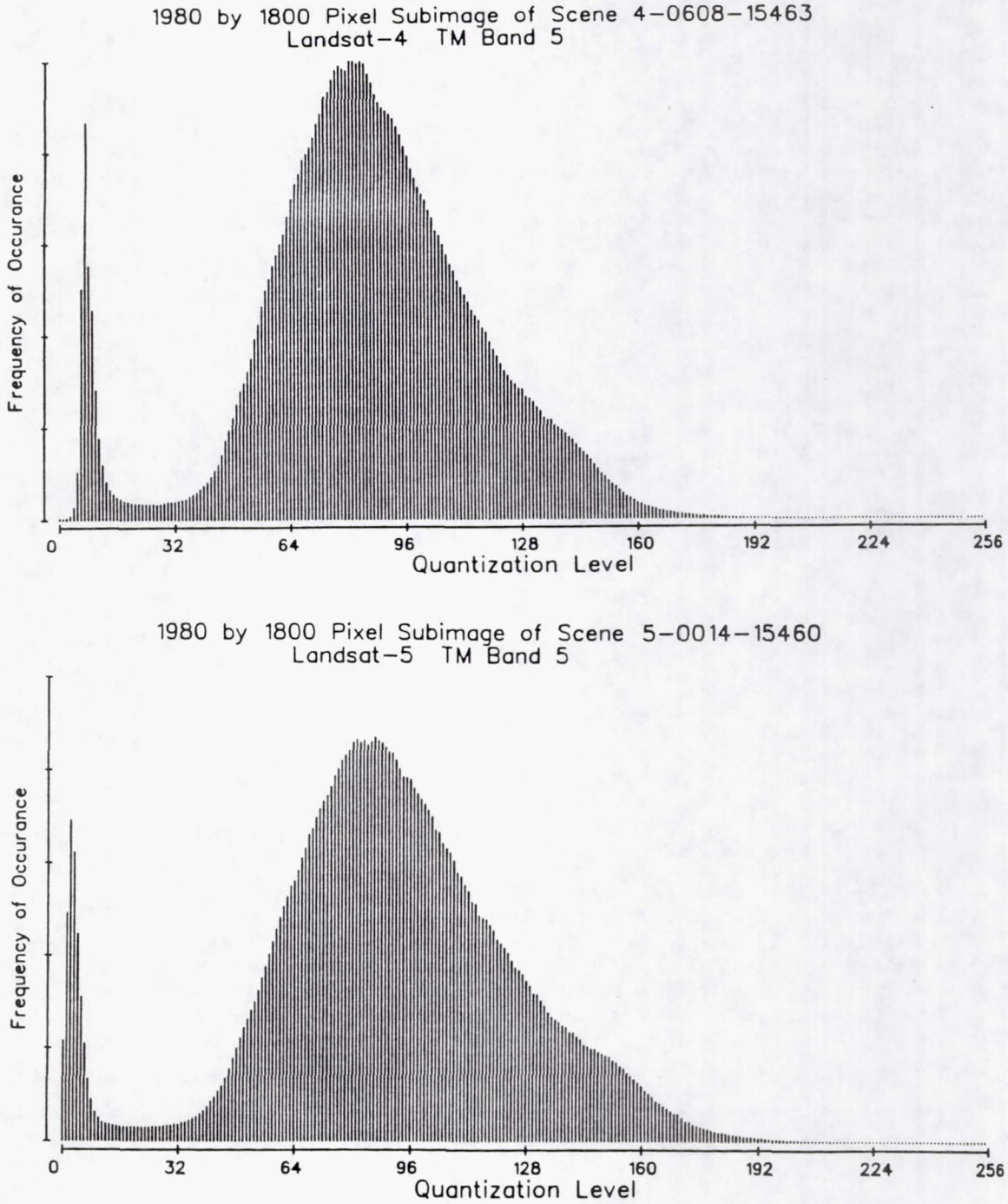

FIG. 8. Landsat-4 and Landsat-5 TM band 5 histograms for coincident regions.

have varying atmospheric effects in different parts of the scene.

This droop effect should not cause serious problems for most users. However, it can confound attempts to extend signatures from one side of a scene to the other and can introduce banding (stripes 16 lines wide, or 17 lines in geometrically corrected CCT-PT data) at the scene edges. Implementation of the proposed exponential model would require pixel-by-pixel correction and could prove costly in

terms of computation time. It is our understanding that NASA and NOAA will leave it to the individual users to determine the importance of correcting for this effect and actually performing the correction.

Also apparent in Figures 4a–4h are oscillations superimposed on the rise effect. These oscillations are coherent noise found in all reflective bands of both Landsat-4 and Landsat-5. Although quite obvious in these plots derived from nighttime data, the peak-to-peak amplitudes are quite small (<0.75 DN in unfiltered data, <0.05 DN in these smoothed plots) and have not been observed in daytime data. The cause of this approximately 400 Hz (262–264 pixel period) noise is undetermined.

Scan-Correlated Level Shifts

In the Landsat-4 TM data we have examined, type 4-7 scan-correlated level shifts are always present, and the signals often shift states with a regular period. Scan-correlated shifts of type 4-1 are present in most, but not all data, and the type 4-1 pattern tends to remain in one state or the other for several scans of the scan mirror. The peak-to-peak amplitude for each affected detector for each form of the shift is essentially constant in all cases where that form of the noise exists. The phase relationships between the affected detectors also remain constant in all images (i.e., band 7 detector 7 is always in its high type 4-7 state when band 5 detector 8 is in its low type 4-7 state). Figure 14 of Malila *et al.* (1984) illustrated both patterns of level shift for the 16 band 1 detectors of Landsat-4 TM for a night scene. Relative magnitudes and phases are readily apparent from the illustrations. Table 1 provides the quantitative results, giving the magnitude and phase of each level-shift pattern for the 96 Landsat-4 TM reflective-band detectors.

Initial analyses of Landsat-5 TM data indicated a similar effect, but with only one pattern (Malila and Metzler, 1984; Barker 1984). We examined nighttime reflective-band data to provide quantification of the magnitude and phase relationships of the effect. Figure 6 illustrates the level shifts for band 3 of Landsat-5 TM, the band most affected by this noise. The plots were produced by computing the mean signal level for each scan for each detector of each band and by plotting these scan-line means versus the scan number. In these plots, the maximum peak-to-peak amplitude is approximately 0.5 DN. Table 2 contains the quantitative results for the reflective-band detectors of the Landsat-5 TM. It can be seen that nearly all detectors are affected, although the magnitude is very low (<0.1 DN) for many. Band 3 shows the greatest effect although band 2 detector 1 is the single most affected detector with a level shift >0.5 DN. The compares with the maximum shift of 2.0 DN measured for Landsat-4 band 1 detector 4. Several detectors did not display any measurable effect in this scene. They are: band 1 detectors 1, 3, 5, 9, 13, and 15; band 2 detector 4; band 4 detectors 8, 10, 12, and 16; band 5 detectors 2, 4, 7, 10, and 13; and band 7 detectors 1, 2, 5, and 15. As seen in Landsat-4 TM data, patterns of phase and magnitude of the level-shift effect within a band often place the detectors into odd-even groups. As with the within-scan droop, the confounding effect of scene data prevents analysis of this type for band 6. For this band, shutter data may be used to quantify any level shifts but with somewhat lowered precision.

Although these level-shifts are strikingly evident in the nighttime reflective data, where the scene makes no contribution to the observed signal level, they are of the same magnitude in daytime data and even there can cause noticeable striping. The magnitude of these shifts and the large number of scenes in which they occur places a high value on the correction of the effect for some applications. Fortunately, the constancy of the magnitude permits relatively simple correction techniques. Since the level shift remains constant for the entire scan, the shifts are also observable in the shutter data collected at the ends of each scan line. Based on this, several methods of correcting for level shifts have been proposed which appear effective in reducing the effect

Table 3. Coefficients for Converting Landsat-4 DN to Landsat-5 DN (Scenes 4-0608-15463 and 5-0014-15460, 15 March 1984)

Landsat-5 TM = A*(Landsat-4 TM) + B

Band	A	B	S.E.	R^2	Range of Data Values (DN) Landsat-4	Landsat-5
1	1.0438	−3.538	0.151	0.99943	73-109	73-111
2	1.1200	−2.719	0.134	0.99922	26-52	26-56
3	0.9869	−3.678	0.142	0.99975	26-77	22-72
4	1.0030	−4.627	0.078	0.99995	11-92	7-88
5	1.1452	−7.330	0.106	0.99999	6-154	0-169
6	1.0040	−0.711	0.119	0.99956	114-148	113-148
7	1.0923	−6.244	0.054	0.99999	3-86	0-88

Note: If the DN computed for Landsat-5 is <0, substitute 0. If it is >255, substitute 255.

TABLE 4. COEFFICIENTS FOR CONVERTING LANDSAT-5 DN TO LANDSAT-4 DN (SCENES 4-0608-15463 AND 5-0014-15460, 15 MARCH 1984)

Landsat-4 TM = A*(Landsat-5 TM) + B						
					Range of Data Values (DN)	
Band	A	B	S.E.	R^2	Landsat-4	Landsat-5
1	0.9580	3.390	0.145	0.99943	73-109	73-111
2	0.8928	2.427	0.120	0.99922	26-52	26-56
3	1.0132	3.726	0.144	0.99973	26-77	22-72
4	0.9970	4.614	0.078	0.99993	11-92	7-88
5	0.8732	6.401	0.093	0.99999	6-154	0-169
6	0.9960	0.714	0.118	0.99936	114-148	113-148
7	0.9155	5.717	0.049	0.99999	3-86	0-88

Note: If the DN computed for Landsat-4 is >255, substitute 255.

(Barker, 1984; Fischel, 1984; Kogut *et al.*, 1983; Malila *et al.*, 1984; Metzler and Malila, 1983a; Murphy *et al.*, 1984). The general approach is to detect the presence of the shift (normally by looking at shutter data), then to subtract (or add) the known magnitude of the shift to each pixel in the affected scan line.

TM LANDSAT-4 VERSUS LANDSAT-5 RADIOMETRIC COMPARISON

Radiometric matching of the Landsat-4 and Landsat-5 TM sensors was facilitated by the availability of a unique set of radiometrically corrected data collected simultaneously by the two sensors and registered to subpixel accuracy as described above. Same-band images from the two sensors were very similar in appearance, although examination on an image display system required different gain and offset factors to be applied to achieve identical brightness and contrast for each pair of images. Since both the Landsat-4 and Landsat-5 scenes were processed through TIPS (Thematic mapper Image Processing System), it was expected that radiometrically corrected products would have essentially identical corrected signal values for the same scene viewed at the same time. In addition to multiplicative and additive differences, clipping of the Landsat-5 data values was obvious in both bands 5 and 7 at the low radiance end of the dynamic range. The band 7 low-level clipping is apparent from a histogram of signal-level frequency for band 7 for both Landsat-4 and Landsat-5 (see Figure 7). The pixels with values zero to six in the Landsat-4 scene are all mapped to value zero in the Landsat-5 scene. Although the offset was nearly as large for band 5 (see Figure 8), fewer data values actually were clipped (0.3 percent of the scene versus 4.2 percent in band 7).

As noted earlier, band-by-band comparisons were carried out using two different techniques: (1) regression of signal values from the coincident pixels or regions, and (2) regression of signal values associated with specific histogram percentile classes. When clipping was not present, either technique produced essentially the same results. Where clipping was present, regression of matched areas led to smaller additive terms and larger multiplicative terms, a result deemed erroneous after inspecting the histograms. For this reason, coefficients from the histogram matching approach are presented here. Table 3 presents the multiplicative and additive coefficients to convert Landsat-4 TM signal levels to Landsat-5 TM equivalent values; and Table 4 contains the coefficients to convert Landsat-5 signals to Landsat-4 values. It should be noted that while this was a simultaneously collected data set, and therefore nearly ideal for this type of analysis, the correction coefficients presented are valid only if ground processing parameters are not changed. It should also be noted that data which have been clipped as in Landsat-5 bands 5 and 7 can not be retrieved—all the zeroes in Landsat-5 band 7 data will be converted to sixes in Landsat-4 band 7, whereas Landsat-4 band 7 would have recorded the same pixels with signal levels ranging from zero to six. In using these conversion equations, resultant DNs less than zero should be assigned the value zero; DNs greater than 255 should be assigned 255.

Converting the pixel values to radiance levels via

TABLE 5. LANDSAT-4 AND LANDSAT-5 TM RADIANCE CONVERSION PARAMETERS (SCENES 4-0608-15463 AND 5-0014-15460, 15 MARCH 1984)

Radiance = $A0$ + $A1$*DN (mW/(cm^2 sr μm))				
	$A0$ (mW/(cm^2 sr μm))		$A1$ (mW/(cm^2 sr μm))/DN	
Band	Landsat-4	Landsat-5	Landsat-4	Landsat-5
1	−0.1500	−0.1500	0.06024	0.06024
2	−0.2802	−0.2805	0.11750	0.11750
3	−0.1203	−0.1194	0.08061	0.08059
4	−0.1504	−0.1500	0.08143	0.08143
5	−0.0372	−0.0370	0.01081	0.01081
6	0.1232	0.1238	0.00569	0.00563
7	−0.1500	−0.1500	0.00570	0.00568

TABLE 6. LANDSATS-4 AND LANDSAT-5 TM REGRESSIONS OF RADIANCE VALUES (SCENES 4-0608-15463 AND 5-0014-15460, 15 MARCH 1984)

	Landsat-5 TM = A (Landsat-4 TM) + B					
					Range of Radiance Values (mW/(cm^2 sr μm))	
Band	A	B	S.E.	R^2	Landsat-4	Landsat-5
1	1.0435	0.205	0.009	0.99943	1.25–6.11	1.23–6.52
2	1.1196	−0.285	0.016	0.99922	2.76–5.87	2.79–6.28
3	0.9865	−0.297	0.011	0.99975	1.98–6.06	1.67–5.68
4	1.0027	−0.376	0.006	0.99995	0.77–7.33	0.42–6.98
5	1.1452	−0.074	0.001	0.99999	−.03–1.63	−.03–1.79
6	0.9932	−0.002	0.001	0.99956	0.77–0.97	0.76–0.96
7	1.0885	−0.002	0.001	0.99999	−.13–0.34	−.15–0.35

the coefficients provided in the Radiometric Calibration Ancillary Record of the Leader File associated with each band of image data (NASA, 1983) did not resolve the discrepancy observed between the two sensors. Table 5 lists the multiplicative and additive coefficients extracted from tape headers and used in the conversion. Table 6 is similar to Table 3 in that it defines conversion of Landsat-4 signals to Landsat-5 equivalent signals but in terms of radiance instead of signal counts. It is not known at this time why the radiometrically corrected data are not more closely matched.

An additional discrepancy was noted between the previously published band 6 temperature sensitivity range and the range implied by the coefficients listed in Table 5. Using these coefficients to convert the range 0.255 DN to radiance gives a radiance range of 0.125 to 1.575 mW/(cm^2 sr μm), representing an apparent temperature range of approximately 200 to 340°K, not the advertised 260°K to 320°K. This causes an increase in the temperature difference represented by a change of 1 DN. The specified 260°K to 320°K temperature range actually spans approximately 63–196 DN versus the specified 0.255 DN. For Landsat-5 TM, the radiance range is very slightly different (0.124 to 1.560 mW/(cm^2 sr μm)), still giving a range of apparent temperature of approximately 200°K to 340°K (or a DN range of approximately 63–193 for apparent temperatures of 260°K to 320°K). Users unaware of these differences may incorrectly derive temperatures from TM band 6 data.

SUMMARY

Landsat-5 TM image data were found to be quite similar to Landsat-4 TM data, both in terms of high overall quality and in the presence of several anomalies. Detailed analysis revealed a systematic within-scan drift (or droop/rise) of the signal from the scene mean toward the overall scan-cycle mean in spectral bands 1 through 4. The magnitude of this drift ranged from minus 1.5 DN (daytime) to +0.15 DN (nighttime), depending on scene content. The drift was fitted with a simple exponential decay model and found to have a time constant equivalent to about one-sixth of a frame width.

Scan-correlated level shifts are present in both Landsat-4 and Landsat-5 TM data. The maximum effect observed in Landsat-5 data was approximately 0.5 DN peak-to-peak, compared with a maximum of 2.0 DN observed in Landsat-4 data. The level-shifts appear to be present in most if not all images, and effective correction procedures have been proposed.

Although data from both Thematic Mappers are produced in radiometrically corrected form, comparison of data acquired simultaneously by the two sensors revealed significant differences in their calibration. In the reflective bands, the multiplicative factors required to convert Landsat-4 TM data to Landsat-5 data ranged from 0.987 to 1.145, with corresponding additive terms of −2.7 DN to −6.2 DN, and displayed evidence of low-level clipping in Landsat-5 bands 5 and 7. The thermal bands (band 6) were more closely matched, but are calibrated to have a full-range temperature range of 200°K to 340°K instead of the advertised 260°K to 320°K.

REFERENCES

Barker, J. L., 1984. Relative Radiometric Calibration of Landsat TM Reflective Bands: *LANDSAT-4 Science Investigations Summary*, v. 1, July, pp. 140-180.

Barker, J. L., Abrams, R. B., Ball, D. L., and Leung, K. C., 1983. Radiometric Calibration and Processing Procedure for Reflective Bands on Landsat-4 Proto-flight Thematic Mapper: *Proceedings of Landsat-4 Science Characterization Early Results Symposium*, v. II, NASA Conference Publication 2355, p. 75.

Fischel, D., 1984. Validation of the Thematic Mapper Radiometric and Geometric Correction Algorithms: *IEEE Transactions on Geoscience and Remote Sensing*, v. GE-22, no. 3, pp. 237-242.

Kieffer, H., Cook, D. A., Eliason, E. M., and Eliason, P. T., 1985. Intraband Radiometric Performance of the Landsat Thematic Mappers: *Photogrammetric Engineering and Remote Sensing*, (this issue).

Kogut, J., Lardinat, E., and Fitzgerald, M., 1983. An Analysis of New Techniques for Radiometric Correc-

tion of LANDSAT-4 Thematic Mapper Images: Research and Data Systems, Inc., Lanham, MD.

Malila, W. A., Metzler, M. D., Rice, D. P., and Crist, E. P., 1984. Characterization of LANDSAT-4 MSS and TM Digital Image Data: *IEEE Transactions on Geoscience and Remote Sensing*, v. GE-22, no. 3, pp. 177-191.

Metzler, M. D., and Malila, W. A., 1983a. Radiometric Characterization of Thematic Mapper Full-frame Imagery; in *Proceedings SPSE/ASP Conference on Techniques for Extraction of Information from Remotely Sensed Images*, Rochester, NY.

———, 1983b. Scan-angle and Detector Effects in Thematic Mapper Radiometry: *Proceedings of Landsat-4 Science Characterization Early Results Symposium*, January 1983, v. II, NASA Conference Publication 2355 pp. 421-441.

Malila, W. A., and Metzler, M. D., 1984. *Eighth Quarterly Progress Report for Study of Spectral-Radiometric Characteristics of the Thematic Mapper for Land Use Applications*: Environmental Research Institute of Michigan, Report No. 164000-13-P, October.

Murphy, J. M., Butlin, T., Duff, P. E., and Fitzgerald, A. J., 1984. Revised Radiometric Calibration Technique for LANDSAT-4 Thematic Mapper Data: *IEEE Transactions on Geoscience and Remote Sensing*, v. GE-22, no. 3, pp. 243-251.

National Aeronautics and Space Administration, 1983. Interface Control Document between the NASA Goddard Space Flight Center (GSFC) and the Department of Interior EROS Data Center (EDC) for Landsat-D Thematic Mapper Computer Compatible Tape (CCT-AT, CCT-PT), Revision A: NASA, no. LSD-ICD-105, p. 60.

APPENDIX C

Comparison of the Information Contents of Landsat TM and MSS Data

Comparison of the Information Contents of Landsat TM and MSS Data*

William A. Malila
Environmental Research Institute of Michigan, Ann Arbor, MI 48107

ABSTRACT: A communications-theory approach is taken to analyze the dispersion and concentration of signal values in various data spaces, irrespective of specific class membership. Entropy is used to quantify information, and mutual information is used to measure the information represented by subsets of spectral variables. Several different comparisons of information content are made. These include comparisons of system design capacities, of data volumes occupied by agricultural data in the spaces defined by original bands and by transformed spectral (Tasseled Cap) variables, of the information contents of original bands and Tasseled Cap variables, and of the information contents of TM and MSS for the given agricultural data sets. Also, the effects of sample size, scene content, and quantization level are examined.

INTRODUCTION

IN ANALYSES OF MULTISPECTRAL data sets produced by imaging remote sensing systems, needs arise for comparing the amounts of information provided by individual spectral bands, by various combinations of bands, and by different sensors. Measures based on classification performance or signal variance (e.g., principal component analysis) are commonly used for such comparisons. Classification procedures require knowledge of the identity of the scene elements being imaged and usually involve assumptions on the form of the signal distributions and parametric descriptors of those distributions. A class-independent and nonparametric measure of information content can be described in information-theoretic terms and is used here to analyze and compare digital image data from the Landsat Multispectral Scanner Subsystem (MSS) and from the Thematic Mapper (TM).

C. Shannon (1948) developed entropy measures of the information content of communications signals. Price (1984) and Bernstein, *et al.* (1984) made entropy calculations and comparisons of Landsat data on a band-by-band or component-by-component basis. Malila (1984) developed a procedure that takes into account dependencies among spectral bands and applied it to original and transformed versions of Landsat data; those results are summarized herein and extended to include additional data sets and other considerations.

* This research was sponsored by the U.S. National Aeronautics and Space Administration, Goddard Space Flight Center, Greenbelt, MD, under Contract NAS5-27346.

METHOD

A communications-theory approach is taken to analyze the dispersion and concentration of signal values in various data spaces. Entropy, as defined by Shannon (1948), is used to quantify information. The process of selecting a subset of bands is viewed as the transmission of data through a communication channel in which loss of information may occur, and the mutual information between input and output is used to measure information transfer, i.e., the information represented by the subset.

Several different comparisons of information content are made. These include (1) comparison of TM and MSS system-design information capacities, (2) comparisons of the TM and MSS data-space volumes spanned by the agricultural data in the spaces defined by both original bands and transformed spectral (Tasseled Cap) variables, (3) comparison of the agricultural information content of original bands to that of transformed variables, and (4) comparison of the agricultural information content of TM data to that of MSS. The effects of sample size and varied scene content are examined, as is the effect of coarser quantization.

BASIC INFORMATION CONCEPTS

Shannon defined self information, $I(x_i)$, as a measure of the information associated with knowing the occurrence of a signal state x_i which occurs with probability $P(x_i)$:

$$I(x_i) = \log_2\left(\frac{1}{P(x_i)}\right) = -\log_2 P(x_i) \quad \text{(bits)} \qquad (1)$$

The rarer the event, the greater is the uncertainty about when it will occur and, consequently, the

PHOTOGRAMMETRIC ENGINEERING AND REMOTE SENSING, Vol. 51, No. 9, September 1985, pp. 1449-1457.

0099-1112/85/5109-1449$02.25/0

greater is the information conveyed when it is observed. Entropy, given the symbol H, is the value of self information when averaged over all N possible states of x:

$$H(x) = \sum_{i=1}^{N} P(x_i) \log_2 \frac{1}{P(x_i)} \quad (2)$$

Entropy is at its maximum when all states or cells are equally likely. It can be reduced by decreasing the number of cells occupied, by having a nonuniform distribution or a concentration of observations in the occupied cells, or both.

With two variables, the use of joint and conditional probabilities is necessary:

$$H(x,y) = H(x) + H(y|x) \quad (3)$$

since

$$P(x,y) = P(x)P(y|x) \quad (4)$$

In computing the conditional entropy, the weighting assigned to each information term is the joint probability of the states involved, i.e.,

$$H(x|y) = \sum_{i=1}^{N_x} \sum_{j=1}^{N_y} P(x_i,y_j) \log_2 \frac{1}{P(x_i|y_j)} \quad (5)$$

If we consider x to be the input to a communication channel and y to be the output, we can define the mutual information transferred between them, i.e., $I_M(x;y)$, as

$$I_M(x;y) = H(x) - H(x|y) \quad (6)$$

This equation shows that the mutual information exchanged is the difference between $H(x)$, the information content of the input, and $H(x|y)$, the information loss or uncertainty about x when we are given the output y. When the total information is transferred, $H(x|y) = 0$ and $I_M(x;y) = H(x)$. At the other extreme, when y does not contain any information relatable to x, $H(x|y) = H(x)$ and therefore $I_M(x;y) = 0$, i.e., there is no mutual information. Figure 1 presents a concise graphical summary of these quantities and their interrelationships. Numerical examples are given by Malila (1984).

Multispectral Extension

The above concepts can be extended to multispectral situations by letting the variables x and y become multidimensional vectors X and Y, with $X = (X_1,X_2,\ldots,X_{N_x})$ and $Y = (Y_1,Y_2,\ldots,Y_{N_y})$. Usually, $N_y \leq N_x$. The information transfer achieved by the communication channel is used here in a general sense, to represent both simple selections of spectral band subsets and more complex transformations, such as the Tasseled Cap transformation.

Absolute vs. Relative Information Content

Multispectral sensors produce signals that have a fixed maximum number of signal levels in each spectral band, usually expressed as a number of bits, e.g., six bits for 64 levels in telemetered Landsat MSS bands and eight bits for 256 levels in Landsat TM bands. When the probabilities in the entropy equations are based on all possible combinations of those levels, absolute information measures will result. These would, for instance, be appropriate when absolute radiometric calibration of data is utilized.

Most current uses of multispectral data, however, employ techniques that utilize only relative amplitude information between signals from various scene elements. In these instances, the information resides in the number of spectral cells that are occupied and the distribution of spectral values within them. Malila (1984) developed an expression that gives a relative entropy value, H_R, for any given data set, in terms of counts of occurrences of observations in cells of the spectral space. It is repeated here (for six variables):

$$H_R(X) = \underbrace{\log_2 N_{obs}}_{\text{Information if each observation were in a unique cell}} - \underbrace{\left(\frac{1}{N_{obs}}\right) \sum_{ijklmn} \cdots \sum C_{ijklmn} \log_2 C_{ijklmn}}_{\text{Information loss due to concentration of the observations into a subset of cells}} \quad (7a)$$

where: C_{ijklmn} is the count of occurrences in the cell having Level i in X_1, Level j in X_2, etc.,

and: N_{obs} is the total number of observations in the data set being analyzed.

More briefly,

$$H_R(X) = H_{max} - H_{loss} \quad (7b)$$

It also is informative to divide the total information loss due to spectroradiometric concentration of signals (from Equation 7) into two components, one due to the reduced number of spectral cells which are occupied (below the total possible) and the remainder which occurs when the duplicate observations are not uniformly distributed among those cells, i.e.,

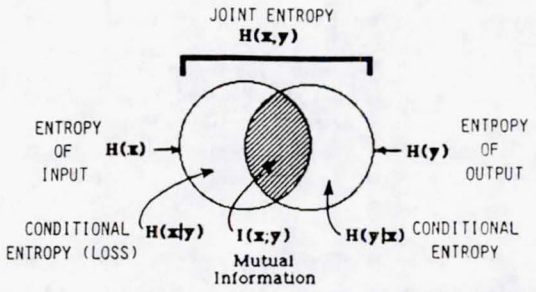

FIG. 1. Summary of Information Relationships.

$$H_{loss} = L_{cell} + L_{unif} \tag{8}$$

where: L_{cell} is the cell loss or loss in number of cells, i.e.,

$$L_{cell} = \log_2 N_{obs} - \log_2 N_{cells} = -\log_2 \left(\frac{N_{cells}}{N_{obs}}\right)$$

and: L_{unif} is the uniformity loss,

$$L_{unif} = H_{loss} - L_{cell}$$

Spectral Band Subsetting

The selection of subsets of spectral bands is a special case of the mutual information expression,

$$I_M(X;Y) = H(X) - H(X|Y)$$

where Y now is a subset, X', of the X variables, so

$$I_M(X;X') = H(X) - H(X|X')$$

Whenever a variable, say X_p, is retained, its conditional probability term becomes unity, its contribution to $H(X|X')$ is reduced to zero, and its information content is retained as mutual information. Whenever a variable, say X_q, is eliminated, there is a loss of mutual information. This loss is represented by the conditional entropy term through all conditional probability components in which X_q occurs on the left-hand side of the conditional probability indicator line but not on the right-hand (or given) side.

Spectral Transforms

Spectral transformations were obtained by applying the linear-combination Tasseled Cap (TASCAP) transformations to MSS (Kauth and Thomas, 1976) and six-band TM (Crist and Cicone, 1984) data. The principal TASCAP variables are Brightness and Greenness. The Brightness variables are positively weighted sums of all bands and respond to general changes in overall scene reflectance. The Greenness variables are essentially contrasts between near-infrared wavelengths (where healthy vegetation is more highly reflecting than soil) and visible wavelengths (where healthy vegetation tends to be less reflecting than many soils) and respond to the amount of vegetation present. These two variables capture 95 to 98 percent of the variability in MSS data from typical U.S. agricultural scenes, while a third variable, called Wetness, has been found to be significant in similar TM data (Crist and Cicone, 1984). The Tasseled Cap variables, though related to principal-component variables, have advantages over them in that the Tasseled Cap directions do not vary with the scene content, and they have more consistent interpretability.

Also, principal-component analysis was utilized to obtain a different set of spectral variables for one comparison. All transformed values were rounded to the nearest integer before being analyzed.

Quantization Effects

To explore the influence of quantization on the resultant information content, the amplitude values were requantized several times. At each step, the number of original digital counts per modified amplitude interval was doubled, thereby compressing the data and reducing the number of bits per channel by one for each step.

DATA SET

MSS and six-band TM data of two types were analyzed. These are (1) real Landsat-4 MSS and TM data acquired simultaneously from an agricultural scene in North Carolina and (2) data values synthesized from field-measured reflectance spectra of agricultural crops and soils using an atmospheric model. These data were used in prior comparisons of the spatial and spectral characteristics of Landsat TM and MSS data (Malila, *et al.*, 1984; Crist, 1984). In the synthetic data, samples are primarily from vegetation at a variety of ground cover percentages, with many fewer examples of bare soil. All analyses of TM data are limited to the six reflective bands; the thermal band was not analyzed in this effort due to its coarser spatial resolution, its dependence on emissive rather than reflective characteristics of scene materials, and lack of a comparable simulation data base. The TM frame was acquired on 24 September 1982 and included a wide range of agricultural crop conditions, ranging from bare soil to green and senescent vegetation to crop residues. It also included some samples from water and vegetation along the Atlantic Coast and from deciduous and coniferous trees.

RESULTS

Spectral Data Volumes

The diagram in Figure 2 helps describe the various terms used here to designate spectral dataspace characteristics, while Table 1 quantifies many of the observed values. Figure 3 presents information measures for several of those quantities, as a function of the number of data variables. First, the

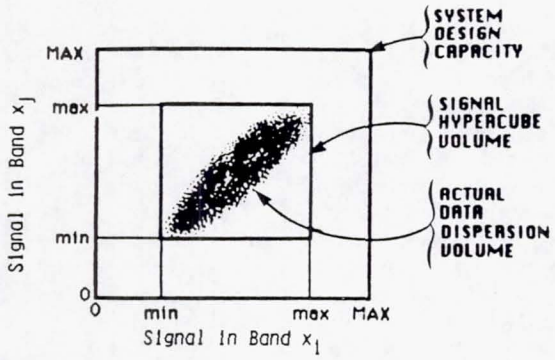

FIG. 2. Illustration of Various Spectral Data Volumes.

system-design capacities of the Landsat-4 TM and MSS are presented in terms of the number of bits transmitted to the ground and/or recorded on computer-compatible tapes (CCTs). For TM, the number of bits recorded on CCTs is the same as that transmitted (8 bits/channel). For MSS, however, the six-bit telemetered data are expanded to seven bits on the CCTs, with only an apparent gain of information. Nevertheless, many comparisons involving MSS will use seven-bit data since that is the form in which we received them. For some others, a degradation to six bits was performed before analysis. The greater information potential of the TM system design (reflective bands), as compared to the MSS system, is quantified as 48 vs. 24 bits in telemetered data.

Figure 3 also portrays the hypercube volume or data-space volume spanned by the TM and MSS data of Table 1a. These volumes are computed by summing the bit equivalents of the observed data-value ranges (max − min + 1) in each band being considered. Upon comparing the fractions of their total data-space volumes that are spanned by data from the agricultural scene, one observes that the TM data fall nine bits short of capacity while the MSS data fall approximately six bits short of capacity.

Actual data dispersion volumes or relative entro-

TABLE 1. INFORMATION COMPARISON FOR MSS AND SIX-BAND TM DATA SETS

A. Values for Real Agricultural Data
(A common area from the N. Carolina scene)

		MSS		Six-Band TM		TM Gain
		number	bits	number	bits	bits
System capacity:	Sensor	0.17×10^8	24	0.28×10^{15}	48	24
	CCT	0.27×10^9	28	0.28×10^{15}	48	20
Hypercube vol.:	Sensor	0.44×10^6	18.7	0.43×10^{12}	38.6	20
	CCT	0.32×10^7	21.6	0.43×10^{12}	38.6	17
Data dispersion pattern:						
	• # Observations; H_{max}	3,468	11.8	13,015	13.7	1.91 (Spatial)
	• #Unique cells	2,898	—	12,903	—	
MSS CCT: 7 bits per band	• Relative Entropy, H_R	—	11.4	—	13.7	2.27 (Total)
	• Entropy loss due to spectral concentration, H_{loss}	—	0.38	—	0.02	0.36 (Spectral)
MSS Sensor: 6 bits per band	• # Unique cells	1,730	—	12,903	—	
	• Relative Entropy, H_R	—	10.3	—	13.7	3.34 (Total)
	• Entropy loss due to spectral concentration, H_{loss}	—	1.45	—	0.02	1.43 (Spectral)

B. Values for Synthetic Agricultural Data
(Assumes equal spatial resolution)

"System" capacity (MSS: 6 bits/band)		0.17×10^8	24	0.28×10^{15}	48	24
Observed hypercube volume		0.10×10^7	20	0.99×10^{12}	40	20
Data dispersion pattern:						
	• # Observations; H_{max}	2,276	11.15	2,276	11.5	
	• # Unique cells	817	—	2,260	—	
	• Relative Entropy, H_R	—	8.94	—	11.14	2.20 (Spectral)*
	• Entropy loss due to spectral concentration, H_{loss}	—	2.21	—	0.01	

* (TM gain over seven-bit simulated MSS data was one bit.)

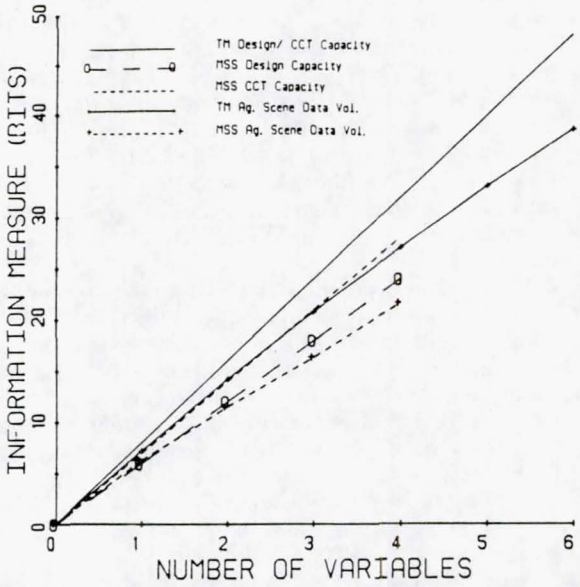

FIG. 3. Comparison of Landsat TM and MSS Information Capacities.

pies (see Figure 2 and Table 1) were found to be substantially smaller than the hypercube volumes, owing to correlations between bands and the limited numbers of observations. Results for the real TM data are shown in Figure 4 and for both TM and MSS (7 bits/band; CCT) in Figure 5. Note that these relative-entropy values for actual information are substantially smaller than those reported by Price (1984) for similar comparisons in which the sum of band values was treated as the joint information content. The data dispersion volumes in Figure 4 are measured by the relative entropies of the best variable combinations, and represent the relative information present in those sets. Most of the information is contained in the first two or three variables. Both the best and worst combinations are shown for each system in Figure 5. The number of observations analyzed establishes a maximum limit on each relative entropy value. As shown earlier in Equation (7), the concentration of multiple observations (pixels) into individual spectral cells reduces the information content below the potential maximum. Table 1 shows very little tendency for TM pixels to do this, owing to the very large system capacity, spectral diversity, and fine gradation of the TM bands. The MSS data show definite tendencies for multiple observations in spectral cells.

Table 1 shows that the TM data represent 3.3 bits more information than the MSS sensor data, with approximately two bits being associated with spatial resolution (pixel size and number) and the remainder with spectral bands and radiometric resolution. Since the synthetic data have the same number of observations for both TM and MSS, they can be considered to have equal spatial resolutions. Thus, the 2.2-bit difference must be solely due to their spectral and radiometric properties.

The above results were for a systematic sample from a larger area, 900 lines by 1300 TM pixels in size (450 × 650 MSS pixels). To explore the effects of sample size and scene content on the information measure, the area was divided into nine subareas, containing varied types and amounts of the scene classes. When all 1.17 million TM pixels were in-

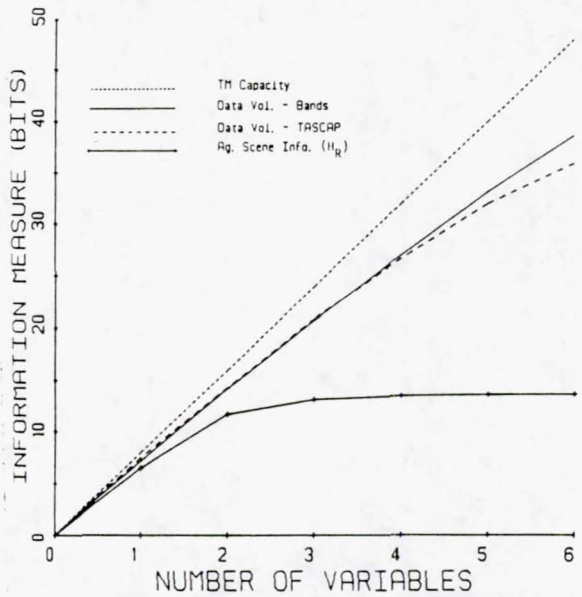

FIG. 4. Thematic Mapper's Utilization of Data Space.

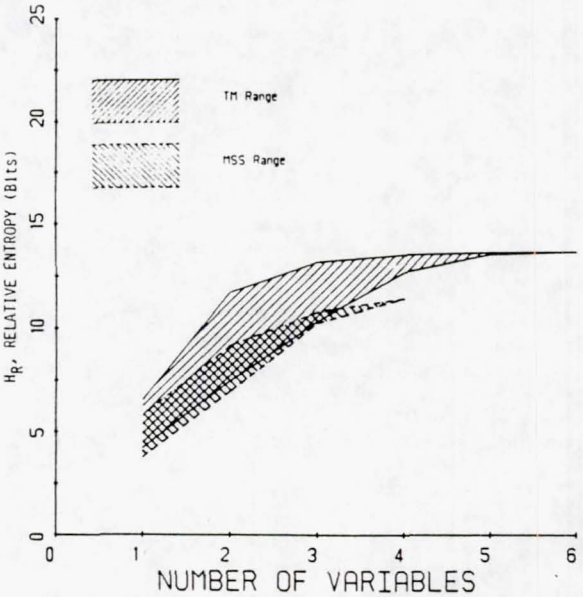

FIG. 5. Range of Information in Subsets of Bands.

cluded in the analysis (Data Set TM-C), an information content equal to 18.4 bits of the possible 20.2 bits was computed, as shown in Table 2. For the corresponding 0.29 million MSS pixels, 13.8 bits of the possible 18.2 bits were present as information. The two bits difference between maximum potentials is due to the greater number of TM pixels. Reductions below the maxima are due to reduced numbers of distinct spectral cells and nonuniformity of the cell populations. Bit equivalents of those losses are also indicated in Table 2. It can be seen that substantially greater losses occur for MSS data than for TM data, leading to a total difference of 4.6 bits between the two data sets.

Values also were computed using all pixels in each subarea. Mean values are given in Table 2 (Data Sets TM-B and MSS-B) along with standard deviations to indicate the amount of variability found among the different scene areas. On the average, both types of losses are reduced from those found in the total data set, but variability among subareas is substantial. Even smaller subsets of data were obtained for analysis by taking every tenth pixel in each subarea; the averages and standard deviations of those values also are listed in Table 2 (Data Sets TM-A and MSS-A). For these, the loss of information by TM is very minor (0.26 bit), but the losses for MSS remain greater (about one bit). Wharton (1984) simulated TM and MSS data sets, analyzed histograms of various sample sizes, and computed ratios of distinct to total number of samples. Comparable numbers were computed from the average cell loss values and are given in the last column of Table 2 as the percentage of cells which are distinct. The percentage for the largest real MSS data set is quite comparable to that for the largest set examined by Wharton, who found 27 percent distinct cells among 230,400 samples. His 59 percent for 28,800 samples and 85 percent for 3,600 samples are higher than the respective 34 percent in Table 2 for 32,500 samples and 66 percent for 3,300 samples. For TM, Wharton found nearly 100 percent distinct cases for even the 230,400-sample case, versus 61 percent here for 130,000 samples, but he considered seven rather than the six dimensions analyzed here and included only samples from nine scene classes. The TM data in Table 2 retain much more distinctness than MSS as the sample size is increased, with 89 percent distinct for 13,000 samples, 61 percent for 130,000 samples, and 58 percent distinct for 1,170,000 samples.

Spectral Transformations

Figure 4 also compares the data-space volumes spanned by original bands and Tasseled Cap transformed versions of signals from the agricultural scene (Table 1A sample). Three fewer bits per pixel are required to provide the same information using the transformed variables than would be required by the original bands. This effect potentially could be used to reduce telemetry requirements; differences might be even greater for data sets with a broader range of scene amplitudes.

For the synthetic MSS data set, a comparison was made of the information content of original band values and two types of transformed variables, TASCAP variables and principal-component variables. They were found to be essentially identical. The equality of the complete sets of variables is in keeping with theoretical considerations of linear transformations.

To compare with the original-band values of Figure 5, relative entropy values for the best and worst TASCAP subsets of each size are presented

Table 2. Effects of Sample Size and Scene Diversity on Information Content

Data Set	Number of Pixels	H_{max} Maximum Possible Relative Entropy (bits)	H_R Actual Relative Entropy (bits)	L_{cell} Loss in Number of Cells (bits)	L_{unif} Uniformity Loss (bits)	$\frac{N_{cells}}{N_{obs}} \times 100$ Percent Distinct Cells+
TM-A	1.3×10^4	13.67	13.41*	0.162*	0.091*	89.4
			(0.21)	(0.136)	(0.078)	[73–99]
TM-B	1.3×10^5	16.99	15.66*	0.711*	0.615*	61.1
			(1.37)	(0.675)	(0.704)	[38–96]
TM-C	1.17×10^6	20.16	18.41	0.791	0.954	57.8
MSS-A	3.3×10^3	11.69	10.72*	0.604*	0.361*	65.8
			(0.47)	(0.331)	(0.148)	[44–88]
MSS-B	3.25×10^4	14.99	12.27*	1.539*	1.179*	34.4
			(1.04)	(0.693)	(0.380)	[16–61]
MSS-C	2.93×10^5	18.16	13.81	2.149	2.200	22.5

* Denotes mean of values from nine subareas.
( ) Denotes standard deviation of those values.
+ Computable from average bits of cell loss, i.e., $100 \times 2 \exp(-L_{cell})$.
[ ] Denotes range of values computed for individual samples.

in Figure 6. In this case, we find an even greater disparity between best and worst combinations, owing to the decreased information content of the last TASCAP variables. Here again, relatively little information is gained by the inclusion of more than three variables.

Dimensionality

Figure 7 displays relative entropy values computed for the first three Tasseled Cap components of TM and MSS data from the agricultural scene (Table 1A sample). (The MSS data were in CCT form at seven bits/band.) The first three components are individually quite similar for TM, but there is a substantial decrease (3.3 bits below Brightness) for the third component of MSS (Yellowness). This is consistent both with many investigators' experiences in finding MSS data of agricultural areas to be primarily two dimensional and with recent studies which have found a substantial amount of information in the TM Tasseled Cap Third Component (Crist and Cicone, 1984). Throughout this comparison, TM values are greater than the corresponding MSS values, for example the TM Brightness value is 6.7 bits compared to 5.8 bits for MSS.

When pairs of components are considered, we see substantial increases in total information, as would be expected with the addition of a second variable; the value for TM Brightness/Greenness is 4.8 bits greater than for Brightness alone, and the corresponding increase for MSS is 3.7 bits. However, differences do appear between MSS and TM. Whereas the value of the Brightness/Greenness pair for MSS is substantially greater than the other two (approximately two bits greater than Greenness/Third Component), there is relatively little difference (less than 0.4 bits) among the three pairings from TM data, pointing to a higher dimensionality in TM.

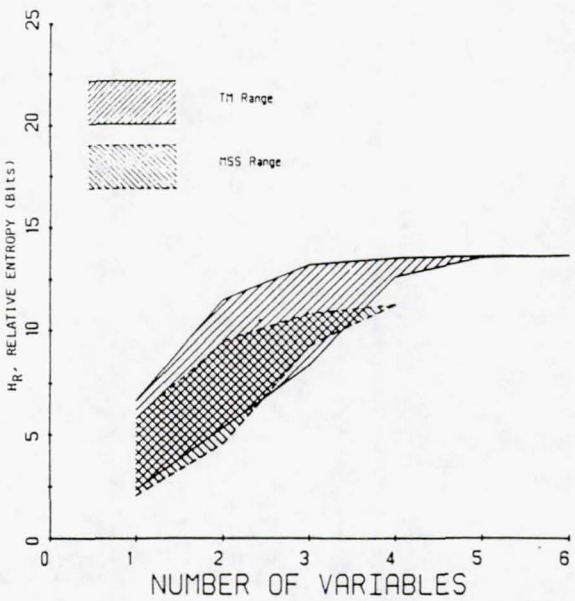

FIG. 6. Range of Information in Subsets of Tasseled Cap Variables.

Three components captured the vast majority of information for both systems. However, the fact that the gain in going from two to three components was nearly as large for MSS (1.25 bits) as for TM (1.70 bits) was somewhat surprising in view of the previously discussed two-dimensional character of MSS data. Furthermore, principal-component analysis of MSS data showed nearly total representation of variance by the first two components. The MSS gain likely is due to the Brightness/Greenness plane having a thickness of several counts in the third direction, even though this third component was uncorrelated with the others. The observed values also indicate that differences do exist among these various measures of multispectral signal properties. The TM data pattern also may be somewhat planar in three space, although not aligned as well with any component axis; correlations with the Third Component were -0.69 for Brightness and 0.36 for Greenness in this data set. None of these observations, however, should diminish the utility of Tasseled Cap transforms for physical interpretation of data values and agricultural scene characteristics.

Noise

Noise in multispectral data was not considered explicitly in the results presented thus far. Sensor noise effects certainly were present in the real Landsat data, and natural variations of crop observations were present in both the real and synthetic data. Noise can add variance to signals and increase the number of spectral cells occupied (above that for no noise), thereby creating an apparent information content greater than the true information content of ideal, noiseless signals. To explore such effects, the number of discrete levels present in the data sets was reduced by applying several different quantization factors (greater than unity) to each band and computing the reduced information content. The results are summarized in Table 3 for three subareas which had (relatively) high, medium, and low information content, respectively. The TM still had more information when degraded to seven bits per band but, by the time the amplitude data were degraded to five bits per band, there was little difference between the corresponding TM and MSS data sets.

SUMMARY

An information-theoretic measure was defined and used to compare Landsat MSS and TM multispectral data. The measure quantifies signal dispersion patterns, independently of class membership and distributional assumptions. It provides an alter-

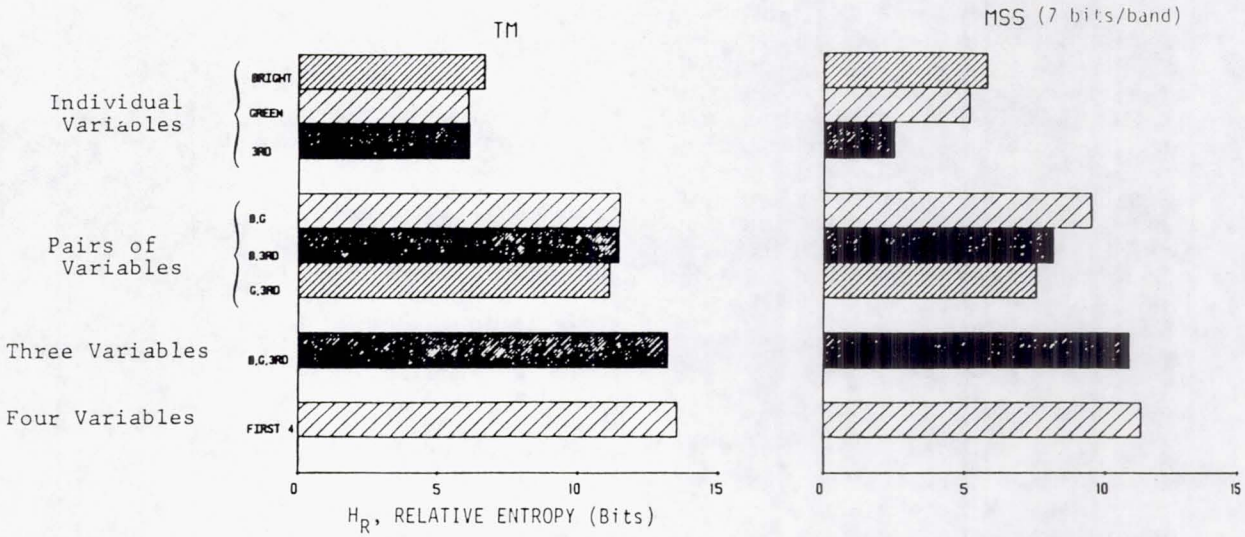

FIG. 7. Comparison of Information Contents of TM and MSS Tasseled Cap Variables.

nate method (to classification) of measuring the extent to which subsets of bands or transformed variables represent the total pattern. The relative entropy value is limited by the number of observations being analyzed. Since results do vary with scene content, analysts should insure that data sets being analyzed are representative of the problems under consideration.

A number of observations were made. The TM system-design information capacity is much greater than that of MSS. The potential information capacities and the signal hypercube volumes of agricultural data were much larger than the information actually represented by signal dispersion patterns in the sets of data values analyzed. Tasseled Cap transformations preserved the information in original bands and offered a modest savings in bits over those original bands, a fact which might be useful in data compression approaches. Relatively few multiple occurrences of spectral observations were found in the TM data sets compared to MSS, another indication of TM's finer partitioning of spectral space. For the best combinations of variables, relative entropy magnitudes were more a function of

TABLE 3. EFFECTS OF QUANTIZATION DETAIL ON INFORMATION CONTENT

Sensor	Number of Pixels	Relative Scene Complexity	Relative Entropy (bits) for Indicated Number of Bits per Band					
			8	7	6	5	4	3
TM	1.3×10^5	High	16.9	15.6	12.3	9.0	6.2	4.6
	1.3×10^5	Medium	16.1	13.4	10.0	7.2	4.8	3.4
	1.3×10^5	Low	15.3	11.8	8.5	5.8	3.7	2.7
MSS	3.3×10^4	High	—	13.8	10.6	9.1	6.4	4.3
	3.3×10^4	Medium	—	12.0	9.9	7.2	4.9	3.3
	3.3×10^4	Low	—	11.0	8.7	6.1	3.8	2.5

Sensor	Relative Scene Complexity	Fraction of Maximum Relative Entropy for Indicated Bits/Band					
		8	7	6	5	4	3
TM	High	1.00	0.93	0.73	0.53	0.37	0.27
	Medium	1.00	0.83	0.62	0.44	0.30	0.21
	Low	1.00	0.77	0.56	0.38	0.24	0.17
MSS	High	—	1.00	0.76	0.66	0.46	0.31
	Medium	—	1.00	0.83	0.60	0.41	0.28
	Low	—	1.00	0.79	0.55	0.35	0.22

the number of variables than of the type of variables (original bands or transformed). TM had greater relative entropy values for Brightness and Brightness/Greenness than did MSS. Information in the Tasseled Cap Third Component of TM was much greater than that of MSS, both by itself and in combination with Brightness or Greenness, confirming TM's greater dimensionality. Reductions in the number of bits used to encode data in each channel decreased the information content, affecting TM data proportionately more than MSS data so that, with five bits or less per band, the information in comparable sets was equal.

REFERENCES

Bernstein, R., Lotspiech, J., Myers, H., Kolsky, H., and Lees, R., 1984. Landsat-4 MSS and Thematic Mapper Data Quality and Information Content Analysis: *IEEE Transactions on Geoscience and Remote Sensing*, v. GE-22, no. 3, pp. 222–236.

Crist, E. P., 1984. Comparison of Coincident Landsat-4 MSS and TM Data Over an Agricultural Region: *Technical Papers of the 50th Annual Meeting of the American Society of Photogrammetry*, v. 2, pp. 308-317.

Crist, E. P., Cicone, R. C., 1984. A Physically-Based Transformation of Thematic Mapper Data—The TM Tasseled Cap: *IEEE Transactions on Geoscience and Remote Sensing*, v. GE-22, no. 3, pp. 256-263.

Kauth, R. J., and Thomas, G. S., 1976. The Tasseled-Cap—A Graphic Description of the Spectral-Temporal Development of Agricultural Crops as Seen by Landsat: Symposium on Machine Processing of Remotely Sensed Data, June 29–July 1, 1976, Purdue University, LARS, W. Lafayette, IN.

Malila, W. A., Metzler, M. D., Rice, D. P., and Crist, E. P., 1984. Characterization of Landsat-4 MSS and TM Digital Image Data: *IEEE Transactions on Geoscience and Remote Sensing*, v. GE-22, no. 3, pp. 177-191.

Price, J. C., 1984. Comparison of the Information Content of Data from the Landsat-4 Thematic Mapper and Multispectral Scanner: *IEEE Transactions on Geoscience and Remote Sensing*, v. GE-22, no. 3, pp. 272-281.

Wharton, S. W., 1984. An Analysis of the Effects of Sample Size on Classification Performance of a Histogram-Based Cluster Analysis Procedure: *Pattern Recognition*, v. 17, no. 2, pp. 239-244.

Malila, W. A., 1984. "Information Theoretic Comparisons of Original and Transformed Data from Landsat MSS and TM". Proceedings of the Eighteenth Int'l Symposium on Remote Sensing of Environment, Oct. 1-5, 1985, (Paris, France), Environmental Research Institute of Michigan, Ann Arbor, MI.

DISTRIBUTION LIST

NASA Goddard Space Flight Center
Greenbelt Road
Greenbelt, Maryland 20771

	Copies
Contracting Officer, Code 284.4	1
Publication Branch, Code 253.1	1
Patent Counsel, Code 204	1
Technical Officer, Mr. Harold Oseroff, Code 902	10